© 2022. Published by The Company of Biologists Ltd | Journal of Cell Science (2022) 135, jcs259289. doi:10.1242/jcs.259289

RESEARCH ARTICLE

A PKC that controls polyphosphate levels, pinocytosis and exocytosis, regulates stationary phase onset in *Dictyostelium*

Shalini Umachandran[1], Wasima Mohamed[1], Meenakshi Jayaraman[1], Geoff Hyde[2], Derrick Brazill[3] and Ramamurthy Baskar[1,*]

ABSTRACT

Many cells can pause their growth cycle, a topic much enriched by studies of the stationary phase (SP) of model microorganisms. Although several kinases are implicated in SP onset, whether protein kinase C has a role remains unknown. We show that *Dictyostelium discoideum* cells lacking *pkcA* entered SP at a reduced cell density, but only in shaking conditions. Precocious SP entry occurs because levels of extracellular polyphosphate (polyP) reach the threshold needed to induce the SP onset at a lower cell density than seen in wild-type cells; adding exopolyphosphatase to *pkcA*$^-$ cells reverses the effect and mimics wild-type growth. PkcA-mediated regulation of polyP depended on inositol hexakisphosphate kinase and phospholipase D. *PkcA*$^-$ mutants also had higher F-actin levels, higher rates of exocytosis and lower pinocytosis rates. Postlysosomes were smaller and present in fewer *pkcA*$^-$ cells compared to the wild type. Overall, the results suggest that a reduced PkcA level triggers SP primarily because cells do not acquire or retain nutrients as efficiently, thus mimicking, or amplifying, the conditions of actual starvation.

This article has an associated First Person interview with the first author of the paper.

KEY WORDS: PKC, Polyphosphate, Stationary phase entry, Postlysosome, Shear stress

INTRODUCTION

Although many organisms can pause their cell cycle, entering either a stationary or a quiescent phase, very little is known about the mechanisms controlling stationary phase (SP) entry in protozoans. A stronger understanding of SP entry in model eukaryotes other than yeasts will reveal whether mechanisms of cell cycle pausing are evolutionarily conserved and provide insights into cell survival under stressful conditions (Brauer et al., 2008). It could also add to insights into cancer biology that have emerged from the pioneering cell cycle research done in yeast (Cazzanelli et al., 2018; Guaragnella et al., 2014; Matuo et al., 2012) and perhaps help in the management of protozoan infections such as malaria.

Different kinases are implicated in SP entry in both bacteria (Jiang et al., 2000; Gaidenko et al., 2002) and yeast (Reinders et al., 1998), but little is known about the role of protein kinase C (PKC). Both entry and survival in SP in *Saccharomyces cerevisiae* are dependent on the serine/threonine kinase Rim15p (Reinders et al., 1998). A cAMP-dependent PKA phosphorylates Rim15p and inhibits its kinase activity, and this inhibited state is necessary for SP entry. This is achieved by increased expression of Bcyl (a regulatory subunit of PKA), which suppresses PKA activity (Werner-Washburne et al., 1991). PKC belongs to a family of serine/threonine kinases and PKC isoforms are known to either promote or suppress cell proliferation depending on the context (Steinberg, 2008). For example, PKCδ inhibits proliferation of vascular smooth muscle cells, but promotes cancer stem cell proliferation in breast cancer cells (Fukumoto et al., 1997; Chen et al., 2014). In many cancer cells, the activation, or inactivation, of a PKC isoform is an important step in signaling pathways influencing cell division, migration, invasion, cell survival and quiescence (Fukumoto et al., 1997; Chen et al., 2014; Kang, 2014; Musashi et al., 2000). In yeast, Pkc1 is required for cell viability and integrity once SP has been entered (Heinisch et al., 1999; Krause and Gray, 2002), but whether it has a role in SP entry in yeast, or in any other microorganism, is unknown.

The model unicellular eukaryote *Dictyostelium discoideum* enters SP and stops dividing after reaching a density of ~2×10^7–2.5×10^7 cells/ml in suspension cultures (Soll et al., 1976; Yarger et al., 1974). Prior to the onset of SP, the concentration of factors controlling proliferation, such as extracellular polyphosphates (polyP), autocrine proliferation repressor A (AprA) and counting factor associated proteins (CfaD) increase, thereby restricting further cell division (Suess and Gomer, 2016; Brock and Gomer, 2005; Bakthavatsalam et al., 2008). As a function of increasing cell density, polyP levels rise, inhibiting further proliferation (Suess and Gomer, 2016). The action of polyP is mediated by the G-protein-coupled receptor GrlD and the small GTPase RasC (Suess et al., 2017, 2019).

Here we show that a putative *Dictyostelium* PKC (*pkcA*; DDB_G0288147), which is also known to have a significant role in multicellular development (Mohamed et al., 2015; Singh et al., 2017) can control SP entry by regulating the rates of pinocytosis and exocytosis, down and up, respectively. This should result in a reduced access to nutrients, thus mimicking or amplifying, the starvation conditions that are the normal trigger for increased extracellular polyP, and SP onset.

RESULTS

Conditional SP defect of *pkcA*$^-$ cells

To determine whether PkcA plays a role in entry into SP, the growth kinetics of wild-type Ax2 and *pkcA*$^-$ cells were examined. Throughout most of the growth phase, the doubling time of *pkcA*$^-$ was significantly higher than Ax2 cells (Fig. 1A). Prior to entering log phase (<1×10^6 cells/ml), the doubling time of Ax2 was 12.5±0.4 h (mean±s.e.m.) compared to 19.0±0.7 h for *pkcA*$^-$.

[1]Bhupat and Jyoti Mehta School of Biosciences, Department of Biotechnology, Indian Institute of Technology-Madras, Chennai 600036, India. [2]Independent Researcher, Write About Research, 14 Randwick St, Randwick, New SouthWales 2031, Australia. [3]Department of Biological Sciences, Hunter College, New York, NY 10065, USA.

*Author for correspondence (rbaskar@iitm.ac.in)

S.U., 0000-0001-6844-0211; W.M., 0000-0002-5553-5569; M.J., 0000-0003-0256-5227; G.H., 0000-0003-0242-8468; D.B., 0000-0003-2652-6230; R.B., 0000-0001-5705-9976

Handling Editor: David Glover
Received 16 August 2021; Accepted 25 March 2022

Journal of Cell Science (2022) 135, jcs259289. doi:10.1242/jcs.259289

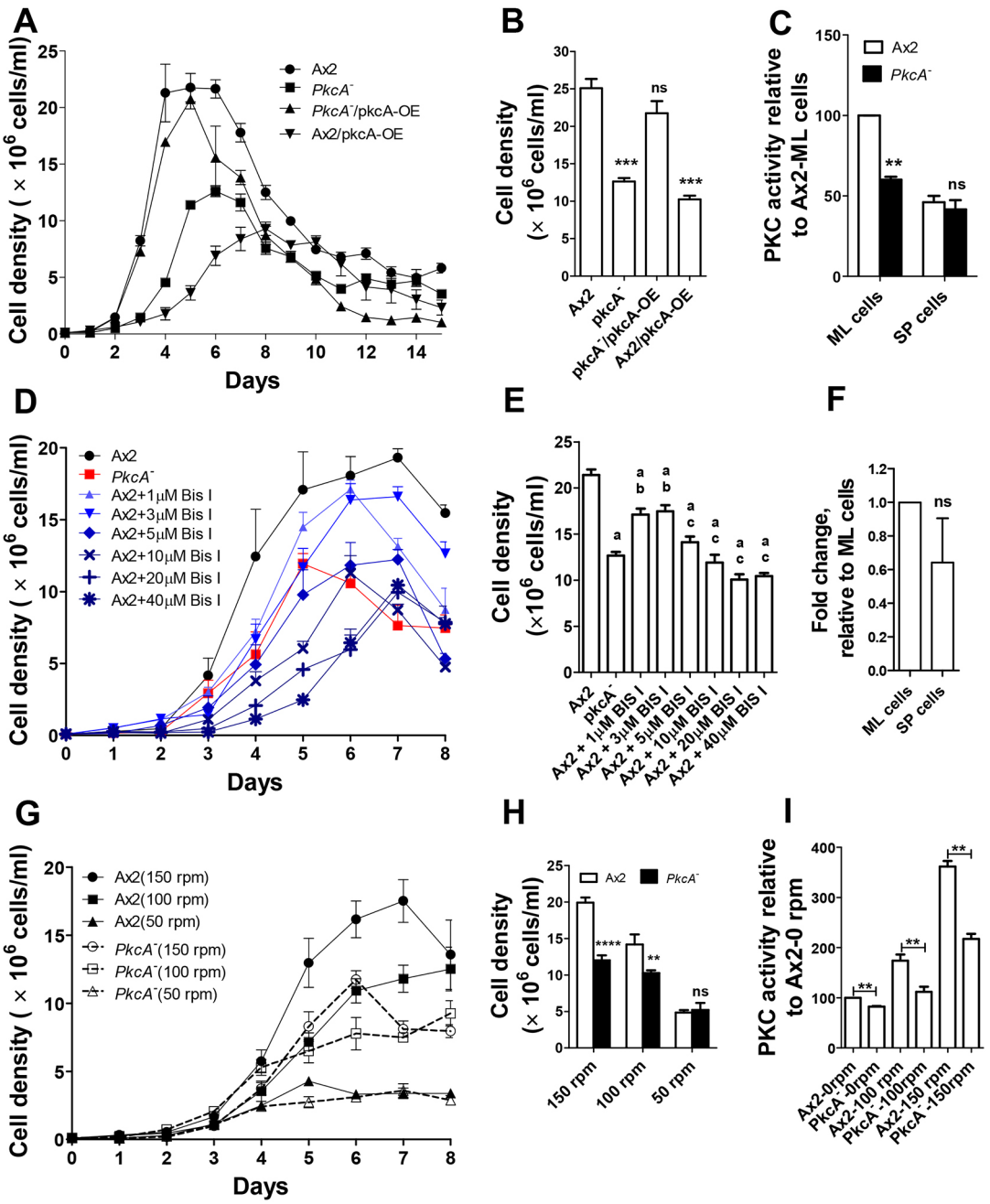

Fig. 1. *PkcA* delays SP onset. (A) Cell proliferation assay was performed in shaking conditions (150 rpm). (B) SP cell density data (from A). The cell densities of *pkcA*$^{-}$, Ax2/*pkcA*-OE and *pkcA*$^{-}$/*pkcA*-OE were compared to those of Ax2. (C) PKC activity assay from mid-log phase (ML) and stationary phase (SP) cells. The activity is normalized to that of ML-Ax2 cells. (D) Dose-dependent effect of the PKC inhibitor Bis I. Ax2 cells were treated with different concentrations of Bis I at an interval of 24 h, and proliferation assays were carried out. (E) SP cell density data (from D); 'a' indicates P<0.001 compared to Ax2, 'b' indicates P<0.001 compared to *pkcA*$^{-}$ and 'c' indicates P>0.05 compared to *pkcA*$^{-}$. (F) qRT-PCR for *pkcA* gene expression in ML and SP Ax2 cells. (G) Cells resuspended at a density of 1×10^{5} cell/ml in HL5 medium were grown at different rpm as indicated. (H) SP cell density data (from G). (I) ML cells were collected from cultures grown at different rpms, and the PKC activity assay was performed. The activity is normalized to Ax2-0 rpm cells. All the experiments were performed three times (n=3) and results are represented as means±s.e.m. ****P<0.0001; ***P<0.001; **P<0.01; ns, not significant [two-way ANOVA with Bonferroni's multiple comparisons (A,D,G,H), one-way ANOVA with Tukey's multiple comparisons (B,E) and paired t-test (C, two-tailed; F,I, one-tailed)].

During log phase growth (1×10^{6}–10×10^{6} cells/ml), the doubling times were 9.8±0.5 h and 14.6±1.1 h, respectively. However, beyond a density of 10×10^{6} cells/ml, the doubling times of Ax2 and *pkcA*$^{-}$ equalized at 18.9±2.0 h and 18.2±0.5 h, respectively. In addition to having a longer doubling time, *pkcA*$^{-}$ cells reached SP at half the cell density of Ax2 cells; 12.6±0.4×10^{6} cells/ml compared to 25.1±1.2×10^{6} cells/ml (Fig. 1A,B; Table S1). Both of the growth defects of *pkcA*$^{-}$ cells were rescued by overexpression of *pkcA*, suggesting that the defects are specifically due to loss of PkcA (Fig. 1A,B). Both defects were also mimicked in Ax2 cells by the addition of a PKC-specific inhibitor [GF109203X; bisindolylmaleimide I (Bis I) (Toullec et al., 1991)] (Fig. 1D,E; Fig. S1B, Table S1) strongly implying that the kinase activity of PkcA is indeed responsible for regulating SP onset.

Individually, either the regulatory or catalytic domain of PkcA failed to rescue the *pkcA*$^{-}$ growth defects, implying that both

Journal of Cell Science (2022) 135, jcs259289. doi:10.1242/jcs.259289

domains are critical for cell density-dependent onset of SP (Fig. S1C; Table S1). The decreased density at which *pkcA*$^-$ cells enter SP was observed in cultures with different inoculum densities and aeration rates, suggesting that this is an intrinsic defect (Fig. S1D,E; Table S1). Interestingly, the growth defects associated with loss of PkcA were not observed when the cells were grown on plates or with bacteria, suggesting that the defect is specific to culturing conditions (Fig. S1F,G).

The *pkcA*$^-$ SP defect only appears in cells experiencing shear stress

As the precocious SP entry of *pkcA*$^-$ cells was only apparent in suspension cultures, we examined whether the shear stress associated with growth in suspension culture played a role in the phenotype. By varying the rotation speed at which the cultures were grown, we found that at a lower speed (50 rpm) the difference in the SP cell density (at SP onset) between Ax2 and *pkcA*$^-$ cells was not significant. However, as the rotation speed increased, the SP-onset densities of Ax2 and *pkcA*$^-$ increasingly diverged (Fig. 1G,H; Table S1). This experiment suggests that PkcA is important for cell proliferation in high shear stress conditions.

PKC activity varies between mid-log and stationary phase cells

Given that the loss of PkcA caused an increased doubling time and precocious SP entry, we examined whether PkcA expression and/or activity varied during cell proliferation in the wild type. Although there was no significant difference in *pkcA* expression in mid-log (ML) cells compared to SP cells (Fig. 1F), PKC activity in SP cells was only 46.1±3.9% (mean±s.e.m.) of that seen in ML cells (Fig. 1C), suggesting that PKC activity decreases when cells are in SP. Our observations are similar to the results reported in neuronal and skeletal muscle cells, which show a significant difference in PKC activity without any change in the expression of PKC isoforms (Rose et al., 2004; Chopra et al., 2018). Interestingly, the PKC activity of *pkcA*$^-$ cells in ML is less than that for Ax2 cells (60.1±1.7% of that in ML Ax2 cells), which suggests the presence of other kinases with similar functions (Fig. 1C). However, the PKC activity drops to 41.6±5.8% in SP *pkcA*$^-$ cells (Fig. 1C). Taken together, these results indicate that lowered PKC activity is associated with low proliferation rates and early SP onset, which is consistent with PkcA activity being involved in their regulation.

Increasing levels of shear stress correspondingly increase PKC activity

Given that (1) the growth defects of *pkcA*$^-$ cells only occur under conditions of high shear stress, and (2) that SP onset and lower proliferation are associated with lowered PKC activity, we examined how the levels of PKC activity in ML cells respond to increased shear stress. Surprisingly, as the shaking speed was increased from 0 rpm to 150 rpm, the PKC activity in both Ax2 and *pkcA*$^-$ cells increased dramatically; the increase was, however, much higher for the wild-type cells (Fig. 1I). Thus, the severity of the defects seen in *pkcA*$^-$ cells do not appear to be related to low absolute levels of PKC activity, but rather correlate with the decreased ability to upregulate PKC activity in response to shear stress.

Conditioned medium from *pkcA*$^-$ cells is potent in inhibiting proliferation

During growth, *Dictyostelium* cells secrete various factors into the medium that control their own proliferation (Bakthavatsalam et al., 2008; Brock and Gomer, 2005; Soll et al., 1976; Yarger et al., 1974; Suess and Gomer, 2016). Thus, the growth defects seen in the *pkcA*$^-$ cells may be due in part to changes in the factors that have been secreted into the growth medium. In order to address this possibility, we grew Ax2 and *pkcA*$^-$ cells until approximately day 5, when both cell types are in SP and examined the effects of replacing the initial growth medium with either: (1) fresh medium (HL5), which will not have any of the extracellular growth factors; or (2) the original growth medium [medium in which the cells were grown until they reached SP; also called conditioned medium (CM)] (Fig. 2A–C). As summarized in Fig. 2A,C (first six bars), both Ax2 and *pkcA*$^-$ cells continued to grow after resuspension in the HL5 medium, and reached SP at a considerably higher density than did either (1) the original pre-replacement cultures, or (2) cultures where the cells were resuspended in their original conditioned media. In the latter case, the Ax2 and *pkcA*$^-$ cells ceased growth. These results clearly support the proposal that secreted factors are responsible for the precocious onset of SP in *pkcA*$^-$ cells.

Next, we repeated the above experiments, except that the cells were resuspended at a quarter of the density used previously and again, the dilution was done on day 5 (Fig. 2B,C, final four bars). In fresh HL5 medium, the cells of both Ax2 and the *pkcA*$^-$ cells continued to grow until they reached the same density as they had before collection (Fig. 2C; compare bars 1 vs 7, and 2 vs 8). However, when the cells were resuspended in their original conditioned media, the cultures did not grow further (Fig. 2C, bars 7 and 8). These results indicate that it is not cell density per se that is responsible for the precocious SP onset, but factors in the growth medium (Table S1).

To further explore the role of the CM as the source of inhibitory factors, we also performed several CM replacement experiments where: (1) the CM from the opposite strain was used (e.g. the Ax2-CM was replaced with *pkcA*$^-$-CM); (2) CM from both ML and SP cultures were tested on ML cells; and (3) finally, after replacement, the cultures were propagated under either high (shaking; Fig. S2A,B) or low (static; Fig. 2D–F) shear stress conditions. The low shear stress experiment was included because, in this case, any effect on growth should only be due to factors secreted into the CM when the culture was exposed, earlier, to high shear stress. When the post-replacement culturing occurred in high shear stress conditions, replacement of the Ax2-CM with the *pkcA*$^-$-CM led to growth inhibition; conversely, replacement of the *pkcA*$^-$-CM with the Ax2-CM led to growth (Fig. 2B). When post-replacement culturing occurred under low shear stress, the same patterns were seen (Fig. 2E,F). The degree of the respective inhibition or stimulation was also greater under high shear stress conditions. As expected, the cell densities observed after replacement with various ML-conditioned media led to higher cell densities than when SP-CM was used (Fig. 2E,F).

Excess polyphosphate levels from *pkcA*$^-$ cells induce early stationary phase entry

A gradual increase in polyP levels during *Dictyostelium* growth eventually leads to the cells entering SP (Suess and Gomer, 2016). Given that *pkcA*$^-$ cells entered SP at a low cell density, we examined whether *pkcA*$^-$ cells also have excess extracellular polyP. For this, the polyP levels in the CM of both Ax2 and *pkcA*$^-$ cells grown in minimal medium (FM) were quantified, as HL5 medium would give background fluorescence (Aschar-Sobbi et al., 2008; Franke and Kessin, 1977). As seen in HL5 cultures, *pkcA*$^-$ cells in FM medium also reached SP at a lower cell density than did Ax2 cells (Fig. S1H). The polyP levels of both the ML and SP-CM *pkcA*$^-$ cultures were

Journal of Cell Science (2022) 135, jcs259289. doi:10.1242/jcs.259289

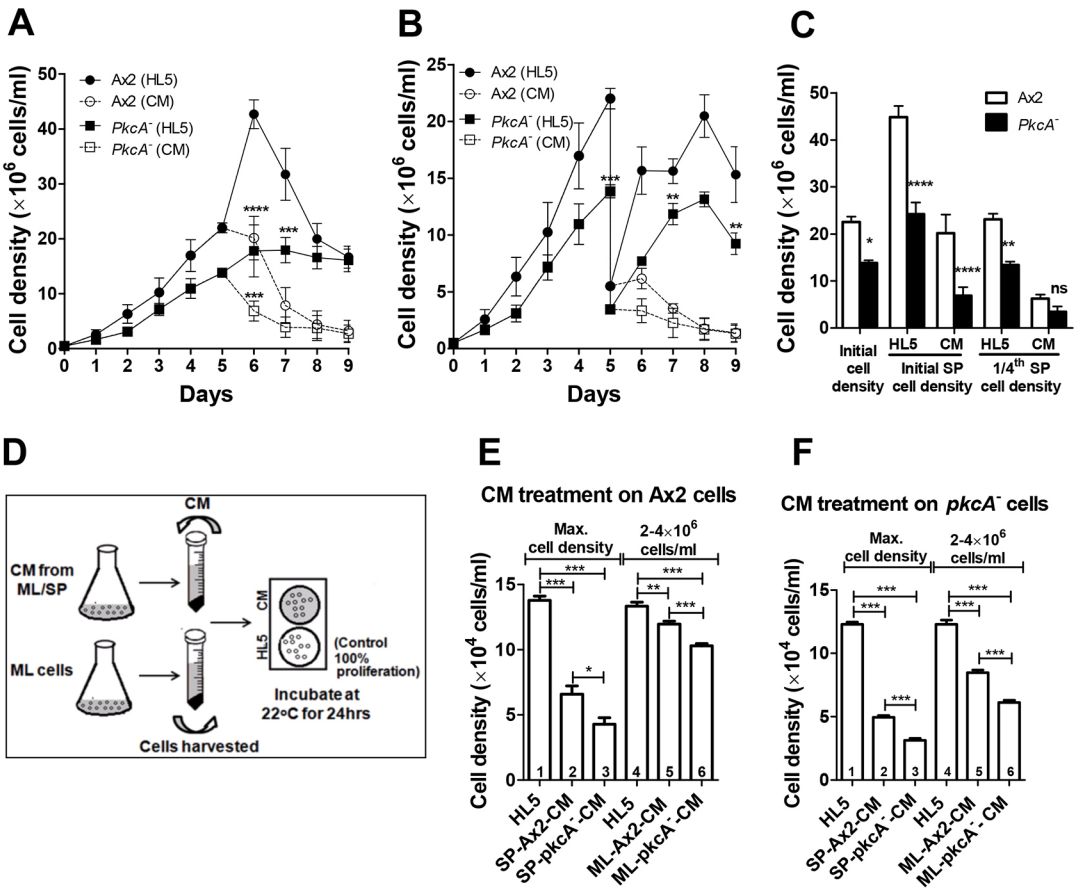

Fig. 2. *PkcA*$^-$ CM inhibits cell proliferation. (A,B) The proliferation assay was performed with SP-Ax2 and SP-*pkcA*$^-$ cells (collected on day 5), resuspended in either in their respective CM or fresh HL5 medium, and cell density was determined daily using a hemocytometer. Cells were resuspended at their respective SP cell density (A) or at 1/4th of their SP cell density (B). For data analysis, *pkcA*$^-$ (grown in CM) and *pkcA*$^-$ (grown in HL5) cells were compared to Ax2 (CM) and Ax2 (HL5), respectively. (C) SP cell density (from A and B). (D) Schematic representation of the experimental design to study the effect of CM. The CM from ML or SP cell culture were collected and added to the ML cells. Cells were treated with 50% CM and 50% HL5. Cells grown in 100% HL5 were considered as a control. (E) The effect of CM on Ax2 proliferation. (F) The effect of CM on *pkcA*$^-$ proliferation. In E and F, bars 1 and 4, control, Ax2 (E) or *pkcA*$^-$ (F) cells grown in HL5; bars 2 and 3, SP-Ax2-CM and SP-*pkcA*$^-$-CM harvested at their respective SP cell density; bars 5 and 6, ML-Ax2-CM and ML-*pkcA*$^-$-CM harvested at ML cell density. Each treatment CM was tested on Ax2 (E) or *pkcA*$^-$ (F) cells, which had been grown in shaking conditions. Data are means±s.e.m.; n=3 biologically independent samples. ****P<0.0001; ***P<0.001; **P<0.01; *P<0.05; ns, not significant [two-way ANOVA with Bonferroni's multiple comparisons (A–C) and one-way ANOVA with Tukey's multiple comparisons (E,F)].

also 1.4 to 1.75 times higher than those of Ax2, while *pkcA*$^-$/*pkcA*-OE (OE, is overexpression) strains had levels similar to the wild type (Fig. 3A,B). The high polyP levels seen in *pkcA*$^-$ appear to be due in part to higher polyP synthesis, as intracellular levels of polyP are also higher than in Ax2 cells (Fig. 3C). Thus, *pkcA*$^-$ cells synthesize and secrete more polyP than wild-type cells.

To determine whether excess polyP is responsible for the inhibitory effects of CM from *pkcA*$^-$ cells, we used the recombinant *S. cerevisiae* exopolyphosphatase ScPPX1, which cleaves polyP (Gray et al., 2014). ScPPX1 treatment (0.15 µg/ml) for 4 h at 37°C (Suess and Gomer, 2016) indeed reduced the extracellular polyP levels in SP-*pkcA*$^-$-CM [56.9±0.1% (mean±s.e.m.) relative to untreated SP-*pkcA*$^-$-CM] (Fig. 3D). Ax2 cells were then incubated for 24 h with ScPPX1-treated and buffer-treated SP-*pkcA*$^-$-CM, and cell density was measured. Consistent with earlier results, buffer-treated SP-*pkcA*$^-$-CM restricted Ax2 growth to 33.7±3.2% of that in the control. Inhibition by ScPPX1-treated SP-*pkcA*$^-$-CM was much less (63.4±0.8% of control level; Fig. 3E). Furthermore, daily addition of 0.15 µg/ml ScPPX1 increased the SP density of *pkcA*$^-$ from 14.0±0.4×10^6 cells/ml to 24.8±2.9×10^6 cells/ml, and Ax2 cells from 19.6±2.3×10^6 cells/ml to 37.5±2.0×10^6 cells/ml (Fig. 3F; Fig. S1I, Table S1). Taken together, these results suggest that *pkcA*$^-$ cells produce excess polyP, significantly contributing to their entry into SP at low cell density.

PkcA controls extracellular polyphosphate levels via I6kA and not Ppk1

The accumulation of extracellular polyP is facilitated by two enzymes, polyphosphate kinase 1 (Ppk1), which catalyzes polyphosphate synthesis, and inositol hexakisphosphate kinase (I6kA), which is involved in synthesis of inositol pyrophosphates (IP7 and IP8) from IP6 (Suess and Gomer, 2016; Zhang et al., 2007; Pisani et al., 2014). The SP-CM from both *ppk1*$^-$ and *i6kA*$^-$ cells had a marginal inhibitory effect on *pkcA*$^-$ proliferation compared to SP-*pkcA*$^-$-CM. On the contrary, SP-*pkcA*$^-$-CM suppressed proliferation in all cell types more than their respective conditioned media (Fig. S2C–F). This suggests that the reduced amount of extracellular polyP in *ppk1*$^-$ and *i6kA*$^-$ cells complements the excess of polyP in *pkcA*$^-$ cells. To identify the particular enzyme through which PkcA controls polyP production, the effect of PKC inhibitor (5 µM Bis I) on the growth of *ppk1*$^-$ and

Journal of Cell Science (2022) 135, jcs259289. doi:10.1242/jcs.259289

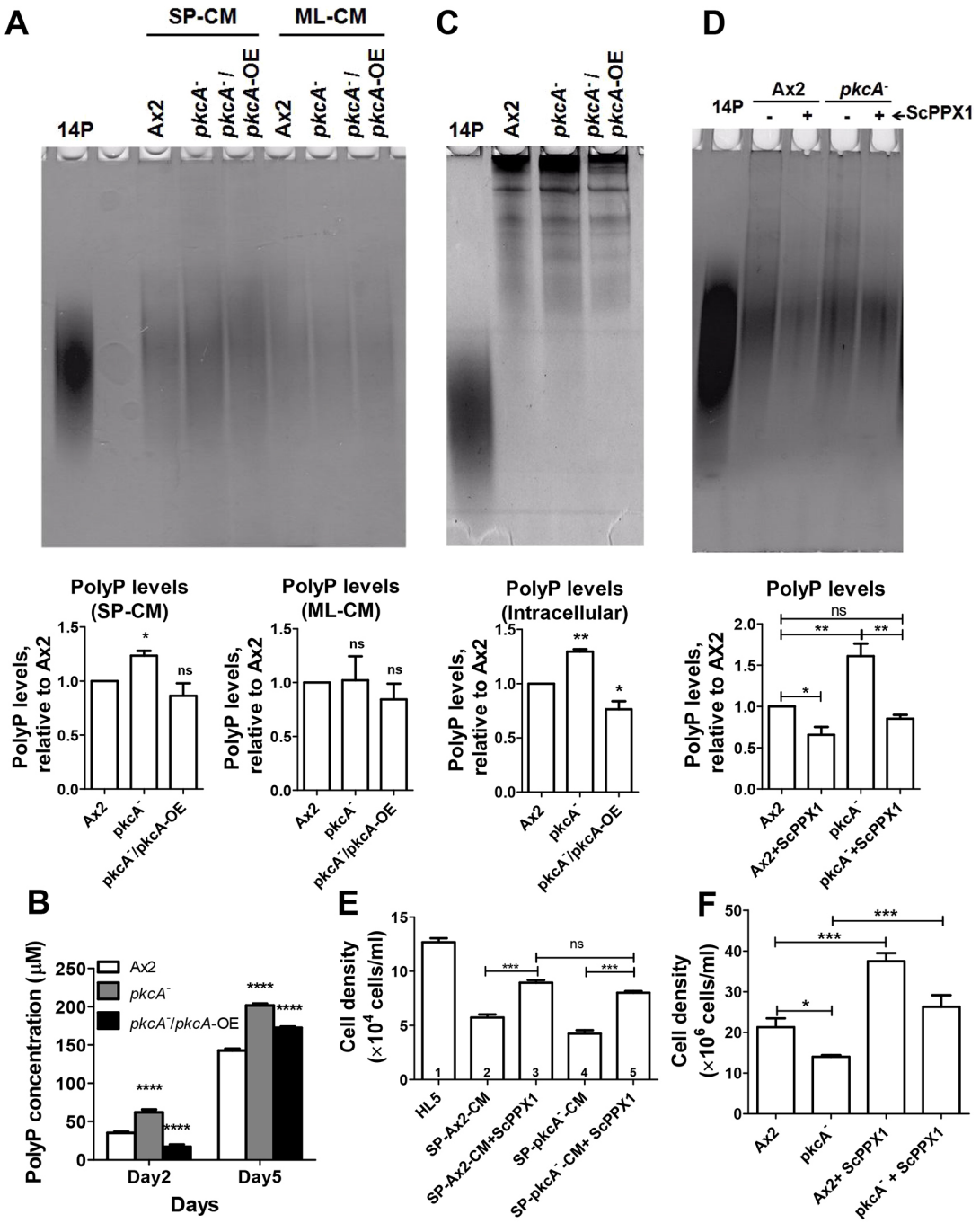

Fig. 3. Excess polyP from *pkcA*$^{-}$ cells causes early SP entry. (A) PolyP from CM (ML and SP) was resolved on a 30% polyacrylamide gel along with 14-mer polyP standard (14P), and gels were stained with Toluidine Blue. (B) Quantification of extracellular polyP concentration in CM (day 2 and day 5). (C) Intracellular polyP was extracted from ML cells, resolved on a 25% polyacrylamide gel. (D) Ax2 and *pkcA*$^{-}$ CM treated cells with ScPPX1 or buffer was analyzed in a 25% polyacrylamide gel. In the case of A,C and D, the polyP levels were quantified from the gel and each value was normalised to that of Ax2 and the image is representative of three experiments. (E) SP-Ax2-CM and SP-*pkcA*$^{-}$-CM cells were treated with 0.15 µg/ml ScPPX1, then ML-Ax2 cells were treated with this CM. Bar 1, control, Ax2 cells grown in HL5; bars 2 and 4, SP-Ax2-CM and SP-*pkcA*$^{-}$-CM cells harvested at their maximum cell density; bars 3 and 5, SP-Ax2-CM and SP- *pkcA*$^{-}$ -CM cells treated with ScPPX1. Each treatment CM was tested on Ax2 cells. (F) Ax2 and *pkcA*$^{-}$ cells were treated with 0.15 µg/ml ScPPX1 or buffer and the SP cell density was estimated. The proliferation curve is shown in Fig. S1I. All the data are means±s.e.m.; *n*=3 biologically independent samples. ***P<0.001; **P<0.01; *P<0.05; ns, not significant (one-way ANOVA with Tukey's multiple comparisons).

i6kA^{-} cells was tested. *ppk1*$^{-}$ cells reached SP at a density of $12.6\times10^6\pm0.6\times10^6$ cells/ml and $27.7\times10^6\pm4.2\times10^6$ cells/ml (mean±s.e.m.) with and without Bis I, respectively. In contrast, Bis I treatment of *i6kA*$^{-}$ cells had no significant impact, with cells entering SP at densities of $35.4\times10^6\pm2.0\times10^6$ cells/ml and $31.9\times10^6\pm1.0\times10^6$ cells/ml in the absence and presence of Bis I, respectively (Fig. 4A,B). Concomitantly, Bis I treatment increased the extracellular polyP levels in SP-Ax2-CM and SP-*ppk1*$^{-}$-CM but had no effect on polyP levels in SP-*i6kA*$^{-}$-CM (Fig. 4C). The lack of effect on *i6kA*$^{-}$ cells in both cases argues that *i6kA* is acting downstream of Bis I inhibition. In other words, PkcA requires I6kA to regulate polyP production and cell density-dependent SP entry.

Journal of Cell Science (2022) 135, jcs259289. doi:10.1242/jcs.259289

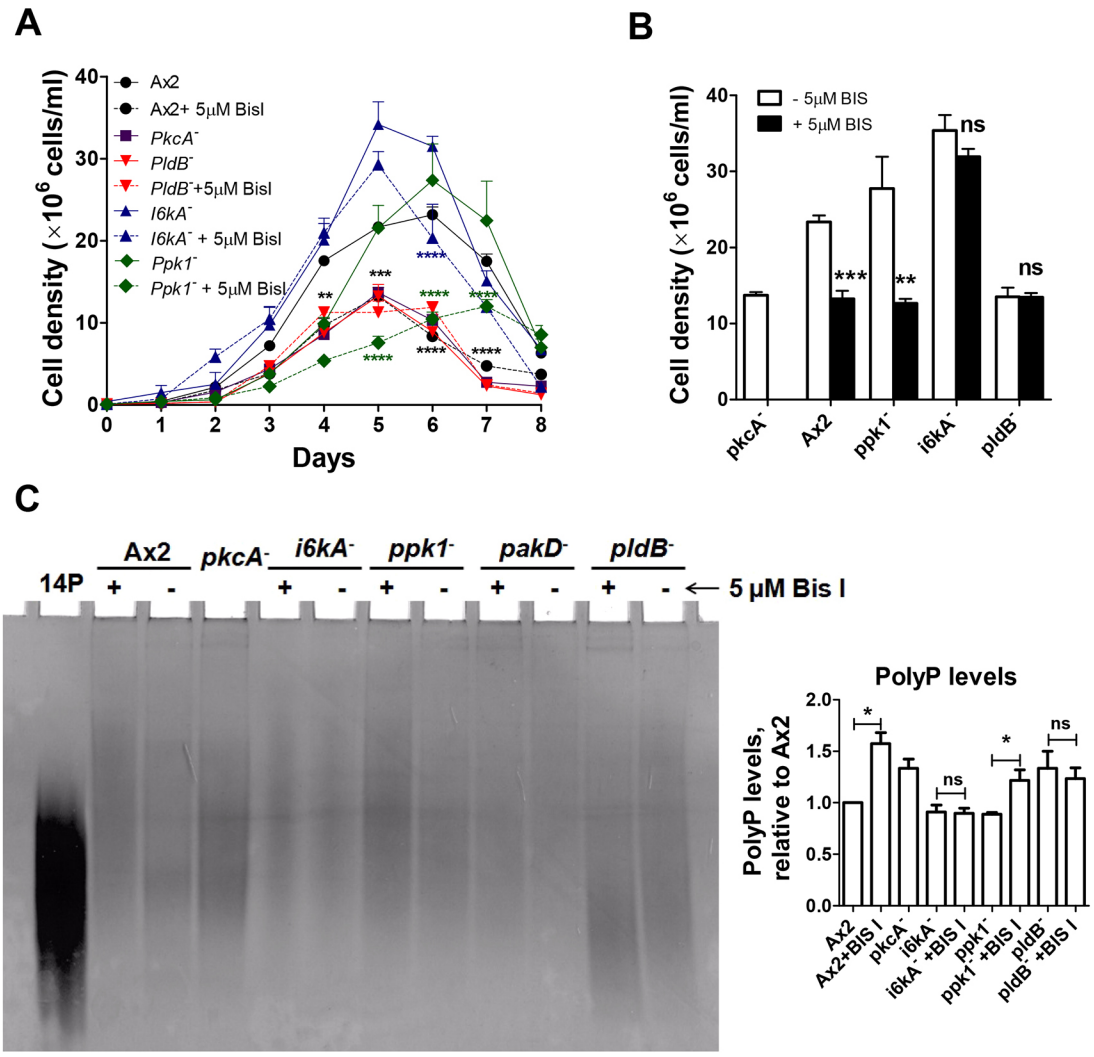

Fig. 4. *pkcA* regulates SP entry via *i6kA* and *pldB*. (A) Proliferation assay of *i6kA*$^{-}$, *ppk1*$^{-}$ and *pldB*$^{-}$ cells treated with 5 µM Bis I or DMSO daily. (B) SP cell density data (from A). (C) The indicated strains were treated with Bis I or DMSO during growth and SP-CM was analyzed on a 25% polyacrylamide gel along with 14-mer polyP standard and stained with Toluidine Blue. PolyP levels were normalized to Ax2 levels. Data are mean±s.e.m.; *n*=3 biologically independent experiments. ****P<0.0001; ***P<0.001; **P<0.01; *P<0.05; ns, not significant [repeated two-way ANOVA with Bonferroni's multiple comparisons (A), and one-tailed paired *t*-test (B,C)]. The growth kinetics and polyP levels of each strain was compared to the appropriate control not treated with Bis I.

PkcA acts via pldB to control stationary phase entry

Previous studies report that PkcA works through the phospholipase D ortholog PldB during *Dictyostelium* development (Singh et al., 2017). To determine whether this relationship also exists during growth, we examined the effect of Bis I on the growth of *pldB*$^{-}$ cells as well as their ability to produce extracellular polyP. Much like with *i6kA*$^{-}$ cells, Bis I treatment had no significant impact on the growth of *pldB*$^{-}$ cells, with SP densities of $13.5\times10^{6}\pm1.2\times10^{6}$ cells/ml and $13.5\times10^{6}\pm0.5\times10^{6}$ cells/ml in the absence and presence, of Bis I, respectively (Fig. 4A,B). Consistent with this, Bis I treatment had no impact on the extracellular polyP levels in *pldB*$^{-}$ cells (Fig. 4C). Also the inhibitory effect of SP-*pldB*$^{-}$-CM on each of the cell types (Ax2, *pkcA*$^{-}$ and *pldB*$^{-}$) was stronger than SP-*pkcA*$^{-}$-CM (Fig. S2G,H). Taken together, these results suggest that PkcA acts via PldB to regulate polyP production and cell density-dependent SP entry.

The secreted chalones are not responsible for the growth defect in *pkcA*$^{-}$ cells

During *Dictyostelium* growth, secreted factors such as AprA and CfaD slow down cell proliferation once they have reached a threshold concentration (Bakthavatsalam et al., 2008; Brock and Gomer, 2005). Thus, the levels of these factors were determined in *pkcA*$^{-}$-CM. Although AprA levels in the ML-*pkcA*$^{-}$-CM were significantly higher (a 2.1±0.5-fold increase) (Fig. S3A,B), there were no differences in the intracellular levels of either protein in Ax2 and *pkcA*$^{-}$ cells (Fig. S3C,D). This suggests that levels of AprA, but not CfaD, correlate with the high levels of polyP in *pkcA*$^{-}$ cells during growth.

Next, to ascertain if the inhibitory activity of SP-*pkcA*$^{-}$-CM is due to excess AprA, the CM was treated with anti-AprA antibody (1:150) and thereafter, cell proliferation was examined in Ax2 and *pkcA*$^{-}$ cells. Surprisingly, there was no difference in the proliferation rates in both cell types (Fig. S3E). Taken together, our results indicate that high AprA levels in ML-*pkcA*$^{-}$-CM are not responsible for the defective growth of the mutant.

Concentrated growth medium rescues *pkcA*$^{-}$ SP defects by decreasing polyP levels

Dictyostelium cells deprived of nutrients are known to have excess extracellular polyP (Suess and Gomer, 2016). If *pkcA*$^{-}$ cells are

Journal of Cell Science (2022) 135, jcs259289. doi:10.1242/jcs.259289

defective in taking up the available nutrients, then providing them with more nutrients may reverse the phenotype. To address this possibility, we grew Ax2 and *pkcA*$^-$ cells in concentrated medium (2× HL5) and measured their cell density and polyP levels at SP. Growth in 2× HL5 had a small but significant effect on Ax2 cells. In contrast, *pkcA*$^-$ cells, reached SP at drastically higher cell density in 2× HL5 medium (Fig. 5A; Fig. S1J, Table S1). There was also a significant reduction (31.2±7.9%; mean±s.e.m.) in extracellular polyP levels (Fig. 5B). These results suggest that the *pkcA*$^-$ phenotype may be due to a defect in nutrient uptake or sensing.

PkcA$^-$ cells have impaired pinocytosis and exocytosis

Nutrient assimilation and cell growth significantly depend on effective pinocytosis and exocytosis. To determine whether the *pkcA*$^-$ phenotype may be due to impaired pinocytosis or exocytosis, cells grown in shaking HL5 cultures were incubated with the FITC–dextran (2 mg/ml, 70,000 M_r), which was collected at the indicated time points, and the uptake of FITC–dextran was measured using a spectrofluorimeter (492 nm ex/525 nm em). ML *pkcA*$^-$ cells had a reduced pinocytosis rate, resulting in only 56.0±3.0% (mean±s.e.m.) of the FITC-dextran uptake seen in Ax2, at 120 min (Fig. 5C). Interestingly, *pkcA*$^-$ cells had higher exocytosis rates, releasing 50% of the FITC–dextran in 30 min, whereas Ax2 cells took nearly 60 min to exocytose the same percentage of FITC–dextran (Fig. 5D).

The increased exocytosis in *pkcA*$^-$ cells could be due to faster postlysosomal neutralization and release of fluids from endo-lysosomal compartments (Neuhaus et al., 2002; Seastone et al., 2001). To test this, the vesicular pH of fluid phase-harboring compartments was measured (Seastone et al., 2001). In the first 10 min, fluid entry was into the acidic compartments (pH<5) in both cell types. In the subsequent 30 min, FITC–dextran entered the

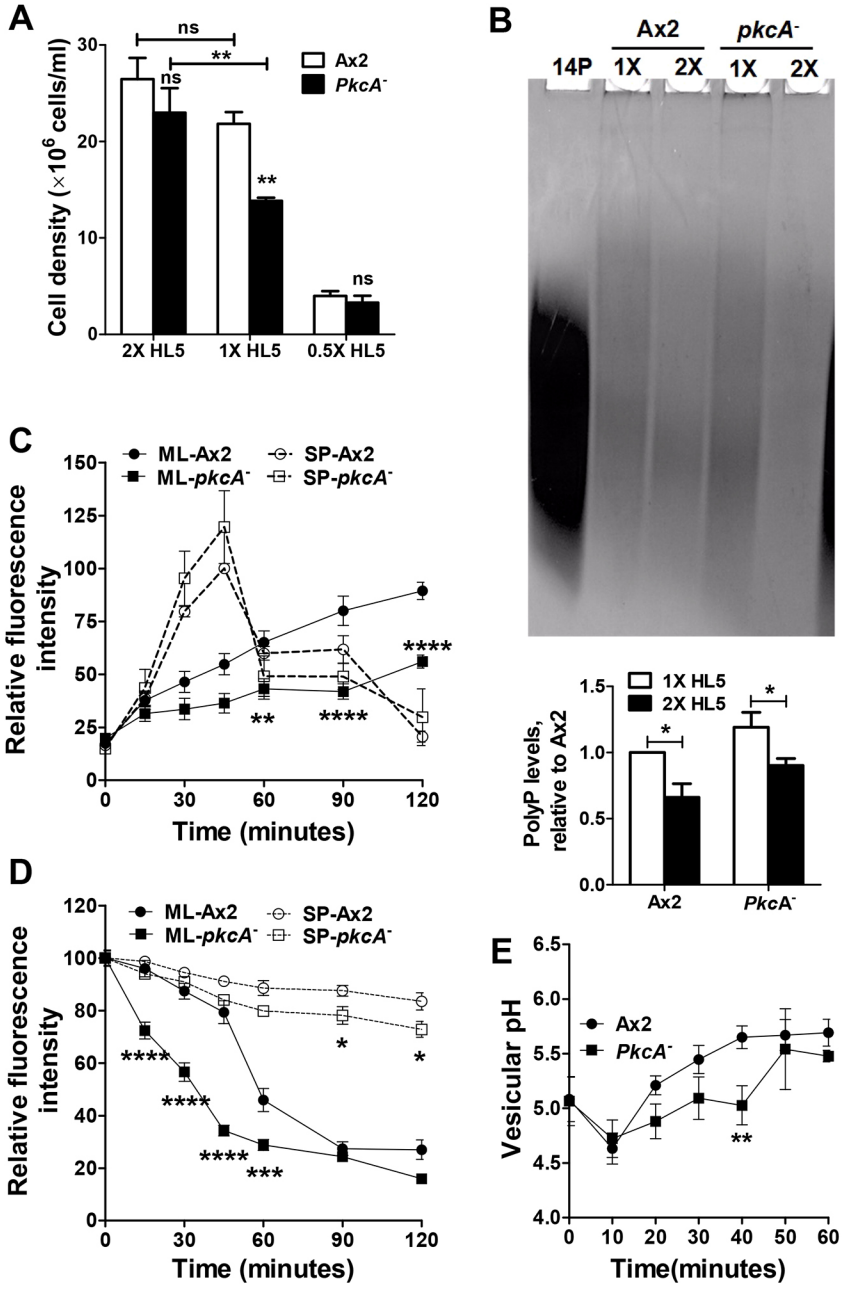

Fig. 5. *PkcA*$^-$ cells are defective in fluid uptake and retention. (A) Cells were inoculated at a density of 5×10^5 cell/ml in concentrated HL5 (2×) and diluted HL5 (0.5×) along with 1× HL5, and SP cell densities were estimated. The growth curve is shown in Fig. S1J. (B) SP-CM from the indicated conditions were resolved in a 25% polyacrylamide gel along with a 14-mer polyP standard and stained with Toluidine Blue. PolyP levels were normalized to Ax2-1× levels. (C) Relative pinocytosis rates. At each time point, the FITC–dextran fluorescence measured in ML cells was normalized to the maximum fluorescence reached by Ax2-ML cells and, similarly, the fluorescence values measured in SP cells were normalized to the maximum fluorescence reached by Ax2-SP cells. Each normalized value was then presented as a percentage. By 45 min the uptake of fluorescent FITC–dextran was higher in SP than ML cells. The relative fluorescent intensity reflecting pinocytosis rates of SP-Ax2 cells were 383.8±67.4% and for SP-*pkcA*$^-$ the value was 461.3±124.3% (mean±s.e.m.) and thus the pinocytosis rates in both cases were similar. (D) Relative exocytosis rates. The fluorescence intensity at *t*=0 was taken as 100% for each condition/strain and for all other time points, the fluorescence was normalized to *t*=0 and presented as a percentage. Although the exocytosis rates were reduced in both cell types, SP-Ax2 cells released just 17% FITC–dextran by 120 min and in the same time period, SP-*pkcA*$^-$ cells released 27% FITC–dextran, suggesting higher exocytosis in the knockout cells, even in SP. (E) Endosomal pH was measured for Ax2 and *pkcA*$^-$ by the dual excitation ratio method. Data are means±s.e.m.; $n\geq3$ biologically independent experiments. ****P<0.0001; ***P<0.001; **P<0.01; *P<0.05; ns, not significant [two-way ANOVA with Bonferroni's multiple comparisons (A,C, D), one-tailed paired *t*-test (B); in E, for each time point the data was analyzed using one-tailed unpaired *t*-test].

Journal of Cell Science (2022) 135, jcs259289. doi:10.1242/jcs.259289

neutral compartments (pH>5.5) of Ax2 cells, but in *pkcA*$^-$ cells, dextran showed a delayed entry into the neutral postlysosomes (PLs) and was detected from 50 min. From this time, the vesicular pH in *pkcA*$^-$ cells (5.5±0.4) was not significantly lower than that of vesicles in Ax2 cells (5.7±0.1) (Fig. 5E). This indicates that rapid postlysosomal neutralization in these cells does not occur, and thus cannot be the reason for the increased exocytosis in *pkcA*$^-$ cells.

Like *pkcA*$^-$, mutants defective in pinocytosis rates have early SP onset

To determine whether low pinocytosis is associated with early SP onset, we measured the cell density at SP of several mutants impaired in pinocytosis or exocytosis. At the same time, the extracellular polyP levels were also quantified. Like *pkcA*$^-$, mutants with reduced pinocytosis rates such as the double-mutant *abpA*$^-$*/C*$^-$ (Rivero et al., 1999), *lvsB*$^-$ (Charette and Cosson, 2007), the double-mutant *proA*$^-$*/B*$^-$ (Temesvari et al., 2000) and *scarA*$^-$ (Seastone et al., 2001), also entered the SP at a low cell density (Fig. S4A, Table S2). Similar to *pkcA*$^-$, *abpA*$^-$*/C*$^-$, *lvsB*$^-$ and *scarA*$^-$ also have high extracellular polyP levels (Fig. S4B, Table S2). Only *proA*$^-$*/B*$^-$ cells had low polyP levels. Taken together, the results point to a significant correlation between defective pinocytosis, high levels of extracellular polyP and entry into SP at low cell density.

Increased F-actin levels in *pkcA*$^-$ cells is associated with increased extracellular polyP levels

The actin cytoskeleton performs important roles during pinocytosis and exocytosis (Seastone et al., 2001; Veltman et al., 2016; Wight et al., 2020). As *pkcA*$^-$ cells have defective pinocytosis and exocytosis, we examined whether F-actin levels or actin assembly were also affected in the mutant. Confocal imaging and SDS-PAGE analysis of the cytoskeletal protein fraction showed higher F-actin levels in *pkcA*$^-$ than in Ax2 cells (1.8±0.2 fold higher) (Fig. 6A,B). Interestingly, in non-shaking conditions, the F-actin levels in Ax2 and *pkcA*$^-$ cells were not significantly different (Fig. 6C) suggesting that PkcA regulates F-actin polymerization differentially in different conditions. The impaired F-actin polymerization in *pkcA*$^-$ cells was observed only when cells were grown in shaking conditions, and such cells were impaired in cytokinesis, were larger and more of them were multinuclear (Fig. S5A–D) (Singh et al., 2017). However, neither myosin II assembly nor its functions were impaired in *pkcA*$^-$ cells (Fig. S6A–D). As polyphosphates are known to affect actin cytoskeleton assembly and polymerization in *D. discoideum* (Suess et al., 2017), and as *pkcA*$^-$ cells have excess polyP, we then examined whether reducing the F-actin levels in *pkcA*$^-$ cells restores extracellular polyP levels and normal growth. This was done by overexpressing coronin A (*corA*), an actin-binding protein involved in F-actin depolymerization (Fig. 6D) (Shina et al., 2011). Overexpression of *corA* in *pkcA*$^-$ cells indeed reduced extracellular polyP levels and restored SP entry, such that it was similar to that in the wild type (Fig. 6E,F; Fig. S1K, Table S1). These results suggest that PkcA, by maintaining actin polymerization, regulates pinocytosis, exocytosis and extracellular polyP levels, thus controlling SP entry.

PkcA colocalizes with lysosomes and regulates postlysosomal size and maturation

Seeking further insights into the cause of the increased exocytosis in the *pkcA*$^-$, we examined subcellular localization of PkcA by imaging vegetative cells expressing a PkcA–GFP fusion protein (Ax2/*act15::pkcA*-GFP). In ML cells, PkcA–GFP was confined to vesicles and the plasma membrane (Fig. 7A; Movie 1), but in SP cells, PkcA–GFP, while largely showing the same distribution, was also partially diffused in the cytoplasm (Fig. 7A). The C1 domain (pkcA-C1–RFP) was only localized to the vesicles; membrane localization was not observed. The catalytic kinase domain (pkcA-cat–GFP) was enriched in the vesicles and also had a diffuse staining in the cytosol (Fig. S7A). The staining patterns suggest that the regulatory C1 domain is important for restricting the vesicle specific localization of PkcA and the full-length protein is important for plasma membrane localization. Confocal imaging also suggests some PkcA–GFP is secreted out of the cells (Movie 2). Extracellular PKC, or any other kinase, would require also the secretion of ATP for its activity; *Dictyostelium* is known to release micromolar levels of ATP into the extracellular environment (Parish and Weibel, 1980; Sivaramakrishnan and Fountain, 2015; Consalvo et al., 2019). Furthermore, we observed PKC localization in lysosomes, the contents of which are known to be exocytosed in other systems (Buratta et al., 2020; Tancini et al., 2020). The CM, which will have all the secreted proteome, shows PKC activity both in ML and SP cells of wild-type and *pkcA*$^-$ cells (Fig. S7B). PKC activity did not affect the localization of PkcA–GFP (Movies 3 and 4). However, F-actin polymerization is important for the movement of vesicles harboring PkcA–GFP (Movies 3 and 5).

To identify the organelles harboring PkcA–GFP, we used MitoTracker RED, which stains mitochondria, and either Acridine Orange (AO) or LysoTracker RED for staining acidic lysosomes. PkcA–GFP did not colocalize with MitoTracker Red (Fig. S7C) but did colocalize with AO- and LysoTracker RED-containing vesicles (Fig. 7B,C). This suggests that PkcA–GFP localization is confined onto lysosomes. Furthermore, PkcA–GFP vesicles colocalized with TRITC–dextran-containing late endosomes (Fig. S7D).

Given the localization of PkcA–GFP on lysosomes and the fact that *pkcA*$^-$ cells show decreased pinocytosis and increased exocytosis, we examined whether the fluid transfer along the endo-lysosomal pathway is defective in *pkcA*$^-$ cells. Ax2 and *pkcA*$^-$ cells were independently incubated with FITC–dextran and AO for 10 min and observed at regular intervals for 1 h using a confocal microscope. Large intense FITC-fluorescent vesicles are known to be less acidic (generally neutral PLs of ∼2 µm diameter) than the smaller vesicles with reduced FITC fluorescence (Seastone et al., 2001). By 60 min, 67.9±1.2% (mean±s.e.m.) of Ax2 cells showed the presence of large FITC–dextran-labeled vesicles with reduced AO fluorescence (less acidic or neutral vesicles) and 35.5±7.7% of *pkcA*$^-$ cells showed vesicles with reduced AO fluorescence (Fig. 7E,F). In the remainder of *pkcA*$^-$ cells, intense AO fluorescence was confined to acidic vesicles. Although the average number of PLs per cell is not significantly different in *pkcA*$^-$ (1.8±0.1) compared to in Ax2 cells (1.9±0.3, P=0.322) (Fig. 7G), *pkcA*$^-$ cells had smaller PLs with an average diameter of 1.2±0.02 µm, whereas, in Ax2 cells, the average diameter of PLs was 1.5±0.03 µm (Fig. 7H). These observations, together with the faster exocytosis rates, suggest the PLs are prematurely exocytosed from *pkcA*$^-$ cells and thus PkcA seems to be involved in regulating the maturation of PLs, and exocytosis. Taken together, the results suggest that PkcA regulates nutrient accumulation and thus cell growth by ensuring that vesicles are retained for an optimal time, such that nutrients can be properly assimilated.

PkcA$^-$ cells have higher protein aggregation

PkcA–GFP is localized in the lysosomes and, given that one of the lysosome-dependent processes, exocytosis, is affected in *pkcA*$^-$

Journal of Cell Science (2022) 135, jcs259289. doi:10.1242/jcs.259289

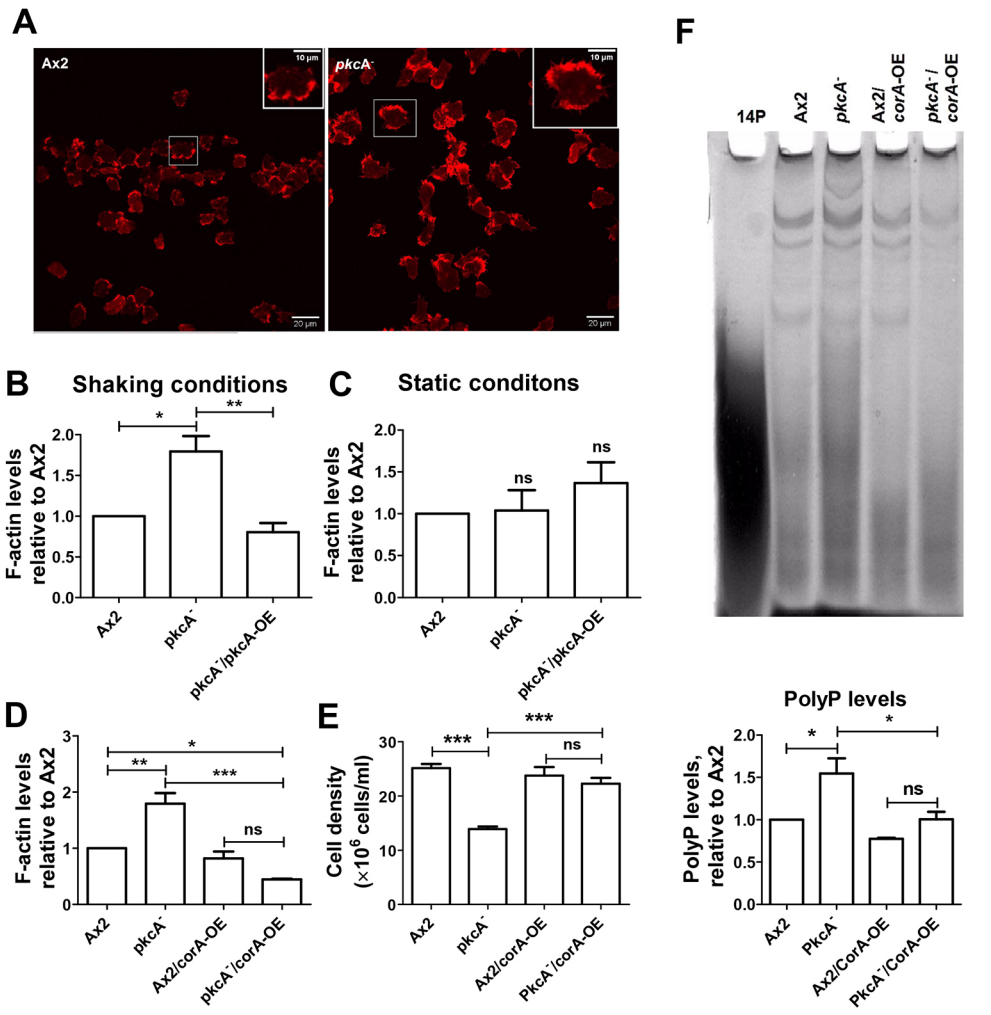

Fig. 6. Increased F-actin levels in *pkcA*$^{-}$ cells are correlated with increased extracellular polyP. (A) ML cells grown in HL5 suspension were allowed to settle on glass coverslips, fixed and stained for F-actin with TRITC–phalloidin. Scale bar: 20 µm. (B–D) Cytoskeletal fractions of cells from shaking cultures (B), non-shaking cultures (C) and *corA*-OE transformed cells grown in suspension (D) were resolved in a 12% PAGE gel and F-actin was quantified using ImageJ, normalized to total protein levels. (E) A proliferation assay for Ax2 and *pkcA*$^{-}$ cells overexpressing *corA* was performed, and SP cell densities were estimated. The proliferation curve is shown in Fig. S1K. Differences between all the values were significant (P<0.0001). (F) SP-CM was resolved in a 25% PAGE gel with 14-mer polyP standard and stained with Toluidine Blue; the image is representative of four experiments. PolyP levels were normalized to Ax2 levels. Data are means±s.e.m.; n=3 biologically independent experiments for all experiments except where mentioned otherwise. ***P<0.001; **P<0.01; *P<0.05; ns, not significant [one-way ANOVA with Tukey's multiple comparisons].

cells, we wanted to ascertain whether any other lysosome-involving processes are affected. One such process is the lysosomal degradation of large aggregates of misfolded proteins transported to lysosomes by the autophagy machinery (Jackson and Hewitt, 2016). PKC isoforms localized in the lysosomes have previously been documented to play an important role in clearing protein aggregates (Li et al., 2016). In *Dictyostelium*, which has a Q/N-rich proteome, protein aggregation, while limited, does occur (Malinovska et al., 2015; Santarriaga et al., 2015). To examine whether the clearance of protein aggregates is PkcA dependent, we transformed Ax2 and *pkcA*$^{-}$ cells with a Q103–GFP construct (polyQ-containing exon 1 of human huntingtin with 103 consecutive glutamine residues), to measure protein aggregate formation. Q103–GFP cells form protein aggregates and GFP spots representing polyQ foci that can be identified microscopically. Confocal imaging and subsequent counting of GFP spots suggest that *pkcA*$^{-}$ cells, at both ML and SP, have higher protein aggregation than the corresponding Ax2 cells (Fig. S7E,F). The fraction of ML-*pkcA*$^{-}$ and SP-*pkcA*$^{-}$ cells with polyQ foci were respectively, 4.3±0.8% and 45.8±1.7% (mean±s.e.m.) compared to the Ax2 cells being 1.9±0.2% in ML and 21.5±2.4% in SP. These two observations, the lysosomal localization of PkcA and the fact that *pkcA*$^{-}$ cells had a larger fraction of cells with protein aggregates, are both consistent with the idea that impaired protein aggregate clearance in the *pkcA*$^{-}$ cells is due to defective lysosomal function. However, protein aggregate clearance is also mediated by autophagy (Jackson and Hewitt, 2016), so the relative contribution of these two processes needs to be examined.

DISCUSSION

Upon nutrient deprivation, many microorganisms cease cell division and enter SP (Herman, 2002). No previous work has examined the possible role of PKC in the onset of SP in *Dictyostelium*, or any of the other model microorganisms. In this study, we demonstrate that *pkcA* (a *Dictyostelium* PKC analog) is important for SP entry in conditions of high shear stress. Our results indicate that, in the shift between ML and SP, PKC activity is reduced, and SP onset is accompanied by higher levels of polyP within the cell, and also, perhaps as a direct and/or indirect consequence, in the medium. As previously shown, a high extracellular level of polyP is one of the crucial signals inducing the coordinated entry of *Dictyostelium* cells into SP (Suess and Gomer, 2016; Suess et al., 2017).

PKC activity drops during the ML-SP transition

Multiple lines of our evidence support, or are consistent with, the idea that a lowered level of PKC activity is an important intermediate step in the transition from ML to SP. The most important observations were the early onset of SP in the *pkcA*$^{-}$ cells and the pattern of PKC activity in the wild type during the ML-SP transition. The involvement of PKC and polyP was also demonstrated by the high levels of polyP in the CM of the early-

Journal of Cell Science (2022) 135, jcs259289. doi:10.1242/jcs.259289

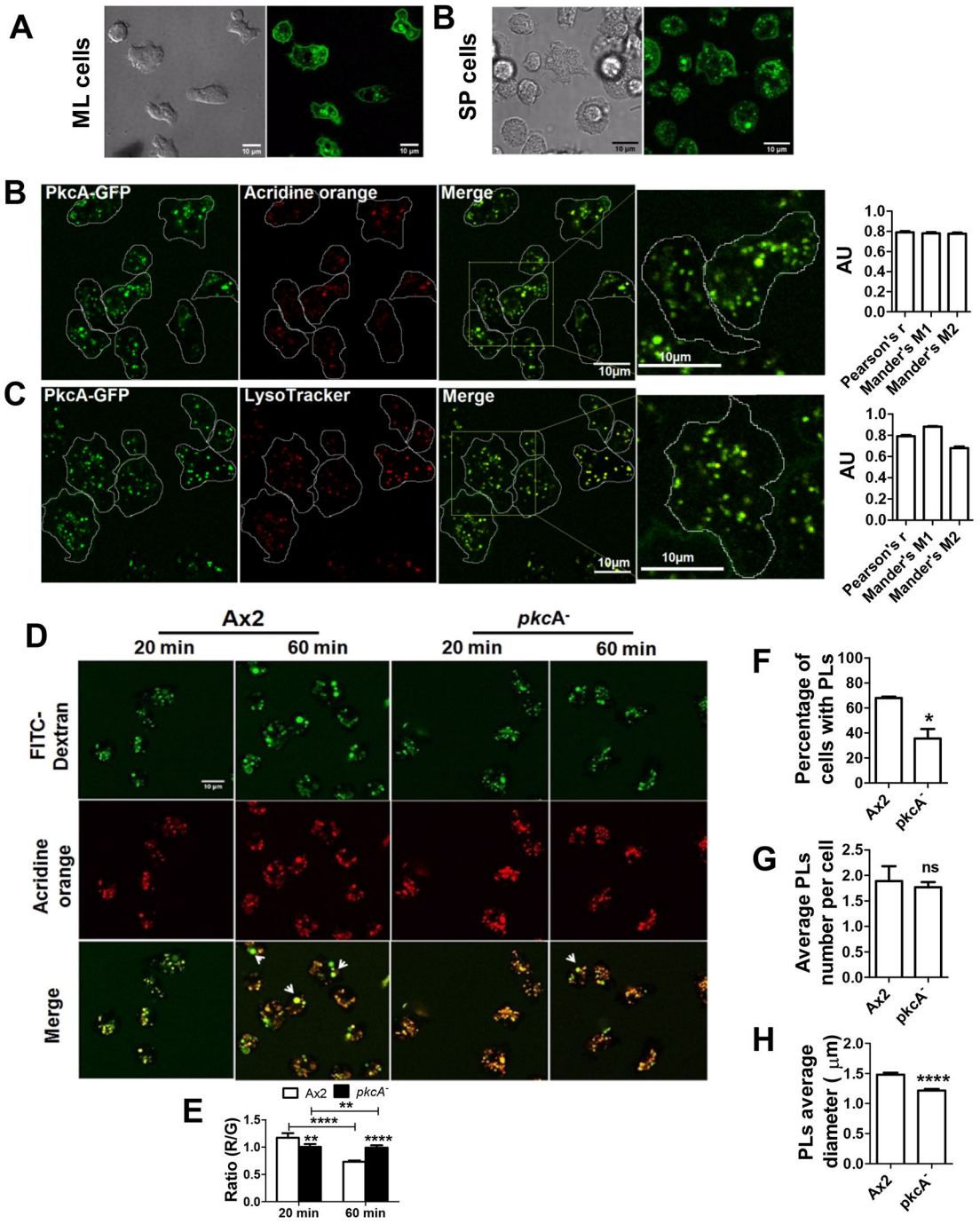

Fig. 7. PkcA–GFP localizes to lysosomes and PkcA regulates PL maturation. (A) PkcA–GFP localization in ML and SP cells. (B,C) PkcA–GFP-containing cells were incubated with 3 µM Acridine Orange (AO) (B) and 200 nM LysoTracker RED (C), respectively. Pearson's correlation coefficient and Mander's overlap coefficient were determined to evaluate the extent of colocalization of PkcA–GFP-containing vesicles with either AO (B) or LysoTracker RED (C). Values are mean±s.e.m. from three independent experiments. (D) Ax2 and *pkcA*$^{-}$ cells were incubated with 2 mg/ml FITC–dextran and 3 µM AO and imaged at the indicated time points. (E) Relative FITC–dextran (green, G) and AO (red, R) fluorescence was estimated. (F) Percentage of cells with PLs for each cell type. At least 50 cells per experiment were examined. (G) Average number of PLs per cell (>50 cells) for each cell type. (H) Average diameter of >100 PLs for each cell type was measured. Data from three experiments were combined for statistical analysis. All values are means±s.e.m. from *n*=3 independent experiments and 30 cells per experiment were examined. ****P<0.0001; **P<0.01; *P<0.05; ns, not significant [paired two-tailed *t*-test (E,H), paired one-tailed *t*-test (F,G)]. AU, arbitrary units.

SP-onset (*pkcA*$^{-}$) line and by the ability of its CM to induce early onset when used to replace the medium of wild-type cells. Although a role for PKC in regulating a microbial cell cycle is novel, PKC is well known to be involved in cell proliferation and cell cycle arrest in many mammalian tissues (Nanos-Webb et al., 2016; Graham et al., 2000; Fukumoto et al., 1997; Chen et al., 2014). In yeast, several Ras proteins, small GTP-binding proteins that activate protein kinase A (PKA) and TOR signaling, are involved in regulating SP entry (Herman, 2002; Werner-Washburne et al., 1991). The onset of SP also involves many kinases, such as Rim15p protein kinase, S6 kinase and PKA (Herman, 2002; Werner-Washburne et al., 1991; Reinders et al., 1998). Both *pkcA*$^{-}$ and

Journal of Cell Science (2022) 135, jcs259289. doi:10.1242/jcs.259289

Ax2/*pkcA*-OE cells show severe growth defects and enter SP at a lower cell density. However, Ax2/*pkcA*-OE cells survive for a longer time in SP (5–6 days compared to 2–3 days for Ax2) suggesting that *pkcA* is important for both SP onset and survival in SP. This is similar to the case in yeast cells, where Pkc1 is required for viability and cellular integrity during nutrient starvation (Heinisch et al., 1999; Krause and Gray, 2002). Thus, either an increase or decrease in *pkcA* levels affects growth. *PkcA* may be regulating different targets at different stages of cell proliferation. For example, both up- and down-regulation of SR-protein specific kinase 1 (SPRK1) promotes cell proliferation in mammalian cells, such as mouse embryonic fibroblasts (Wang et al., 2014).

Reduced *pkcA* leads to increased intracellular and extracellular polyP

Reduced levels of *pkcA* are associated with increased levels of polyP, both intracellularly, and even more importantly, extracellularly. In our model, PkcA drives this relationship and is responsible for regulating polyP levels (Fig. 8A,B). Although it is possible that the reverse is true, and that increased extracellular

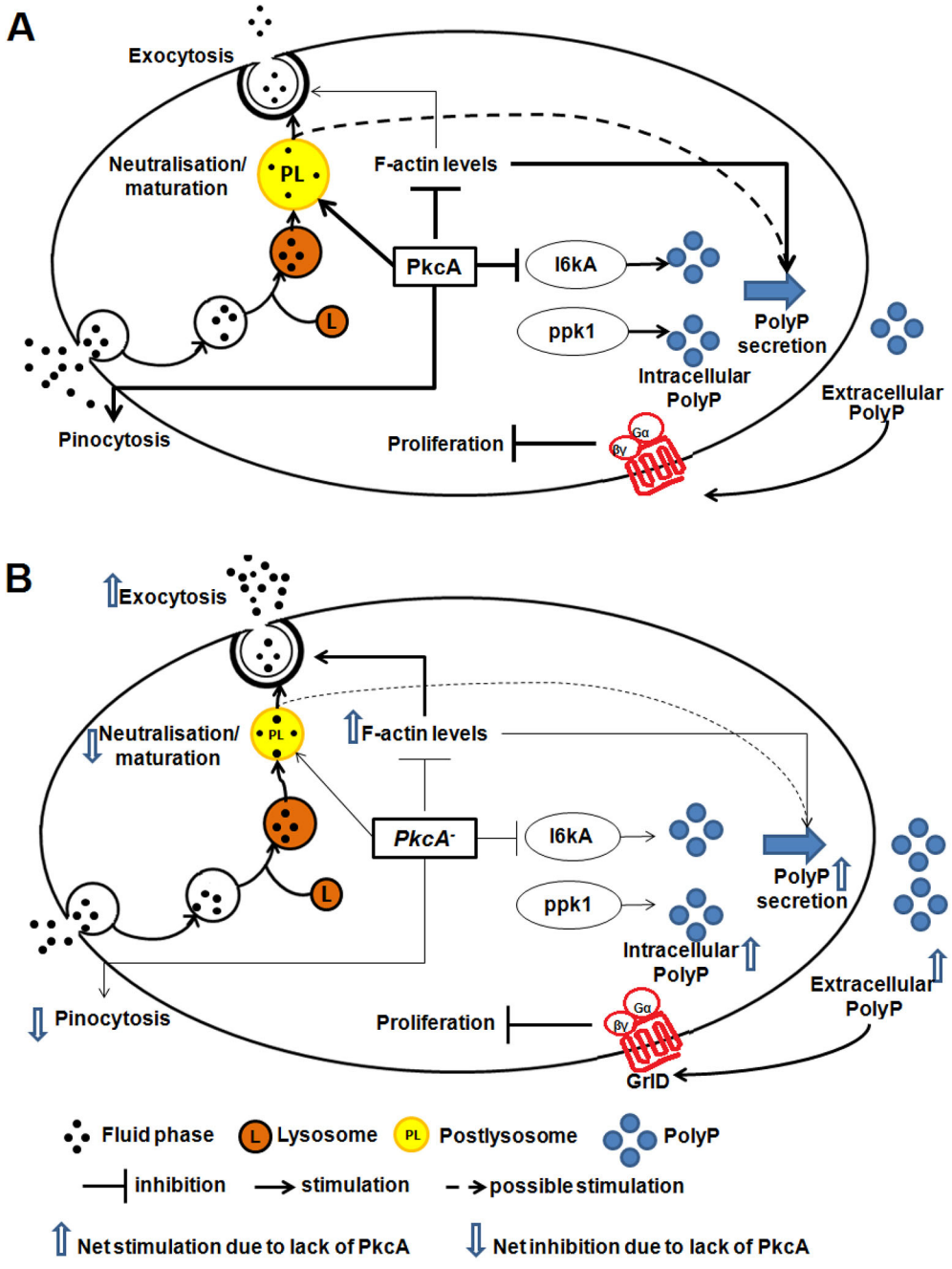

Fig. 8. Pathways regulated by PkcA during cell proliferation. (A) PkcA promotes cell proliferation by suppressing I6kA expression/activity, which in turn reduces polyP levels, a well-known cause of cell proliferation. Furthermore, PkcA reduces F-actin levels, ensuring appropriate levels of pinocytosis, exocytosis and nutrient retention. (B) *PkcA*$^{-}$ cells exhibit decreased pinocytosis and premature exocytosis, thereby nutrients stay in the cell for a shorter time, thus mimicking starvation. In the absence of PkcA activity, both intra- and extra-cellular polyP levels rise. All these defects lead to the onset of SP at a lower cell density. Thick arrows indicate strong stimulation or inhibition, and thin arrows indicate reduced stimulation or inhibition.

Journal of Cell Science (2022) 135, jcs259289. doi:10.1242/jcs.259289

polyP results in lowered *pkcA*, previous proteomics work argues against it (Suess et al., 2017). It should also be noted that polyP at different concentrations (125 µM and 150 µM) suppresses cell proliferation of *pkcA*$^-$ and wild-type cells equally; thus, the sensitivity of *pkcA*$^-$ cells to polyP is similar to that of the wild type, suggesting that *pkcA* is not required for polyP-mediated proliferation inhibition (Tang et al., 2021). Also, of the two genes *i6kA* and *ppk1*, which are involved in regulating extracellular polyP levels (Suess and Gomer, 2016; Zhang et al., 2007), we show that only *i6kA* and *pkcA* are epistatically related, suggesting that they share an enzymatic pathway. We argue that prior to SP, at a low cell density, PkcA inhibits I6kA-dependent polyP production, whereas at high densities, reduced PkcA activity leads to increased polyP production via I6kA. This is the first report suggesting that a PKC regulates I6kA. *PkcA*$^-$ cells had reduced expression of *i6kA* (Fig. S8A). Possibly, I6kA protein activity is either not compromised or the reduced expression is in fact a negative feedback response to increased I6kA activity. Alternatively, even reduced levels of *i6kA* may be sufficient to support the function of the protein. Although the mechanism by which PkcA regulates I6kA is yet to be ascertained, there are two possible PkcA phosphorylation sites (Ser9 and Ser572) in I6kA (Netphos 3.1) (Fig. S8B). Additionally, our work indicates that PldB also acts downstream of PkcA to regulate extracellular polyP levels and proliferation; PldB has previously been shown to interact with PkcA during the development stage of *Dictyostelium* (Singh et al., 2017). Neuronal PLD3 localizes in lysosomes and regulates the structure and function of lysosomes (Fazzari et al., 2017).

Reduced *pkcA* leads to increased actin and changed rates of nutrient exchange

Our work suggests that an important step in the process by which reduced PkcA leads to higher polyP is a rise in actin polymerization. We documented higher levels of actin in the *pkcA*$^-$ line, and showed that when the actin-depolymerizing protein CorA was overexpressed in this line, the extracellular polyP levels of the mutant were lower, and SP onset reverted to that of the wild type. For the following step in our model, that is, disrupted pinocytosis and exocytosis leading to nutrient depletion, we do not have direct evidence that the observed rate changes in the *pkcA*$^-$ line were due to the observed increase in actin levels. However, previous studies on *Dictyostelium* using actin-regulating-protein mutants (such as *scar*$^-$) and drug treatments, such as cytochalasin treatment, have demonstrated the importance of F-actin levels in pinocytosis and exocytosis (Seastone et al., 2001; Wight et al., 2020; Veltman et al., 2016). Similarly, PKC inactivation in neuronal cells is known to induce F-actin polymerization (Yang et al., 2013). In *Dictyostelium*, an increased level of actin does not, however, appear to be an obligatory step in SP onset. Although 2× HL5 rescued the cell density-dependent SP defect of the *pkcA*$^-$ line, the F-actin levels remained high. This implies that nutrient levels can control polyP levels independently of PkcA-regulated actin polymerization. It is also important to note that adding polyP to the growth medium has been reported to lead to lowered actin levels in *Dictyostelium* (Suess et al., 2017).

Changes in pinocytosis and exocytosis rates in the *pkcA*$^-$ mutant

Regardless of whether actin is directly involved, the rates of pinocytosis and exocytosis in the *pkcA*$^-$ were lower and higher, respectively, than in the wild type, and each of these changes is a potential driver of early SP onset. Reduced pinocytosis and increased exocytosis are likely to result in, respectively, less access to, or retention of, nutrients, thus accentuating the starvation conditions associated with rising cell density. The involvement of reduced pinocytosis in polyP-driven SP onset was also supported by the early onset seen in four pinocytosis-defective mutants, three of which also had high extracellular polyP. Furthermore, the rescue of the *pkcA*$^-$ growth defect in concentrated medium (2× HL5) supports the hypothesis that reduced nutrient retention is one of the main features of the *pkcA*$^-$ growth defect.

Exocytosis-defective mutants showed drastic variation in extracellular polyP levels, suggesting exocytosis might not be directly involved in regulating the polyP levels. Rather, in the case of *pkcA*$^-$ cells, increased exocytosis could have resulted in decreased retention time of nutrients, leading to starvation conditions.

PkcA–GFP localization in LysoTracker RED-positive vesicles and at the plasma membrane in *Dictyostelium* does suggest a direct involvement of PkcA in vesicle trafficking, as has also been reported in HeLa cell lines (Li et al., 2016). The C1 domain of PkcA is important for confined vesicular localization. Also, we show that both regulatory and catalytic domains are required to rescue the *pkcA*$^-$ growth defect, consistent with previous observations (Steinberg, 2008). Our study also shows that only 35% of *pkcA*$^-$ cells had neutral PLs of reduced size, indicating that there is a role for PkcA in regulating their maturation.

PL maturation might well be the stage affected by increased levels of actin. In *Dictyostelium*, the actin coat on late endosomes is crucial for PL neutralization and lysosomal fusion leading to exocytosis (Rivero, 2008). Thus, increased F-actin levels in *pkcA*$^-$ cells might be preventing the fusion events necessary for PL maturation, with PLs thus remaining small. Postlysosomal fusion events are necessary for lysosome maturation and, in *pkcA*$^-$ cells, PLs are exocytosed earlier, impairing the fusion events, as observed in *cpnA*$^-$ cells (Wight et al., 2020; De Araujo et al., 2020). In pancreatic β-cells, PKC enhances the exocytosis of insulin by causing the rearrangement of cortical actin, and phosphorylation of exocytotic proteins (Trexler and Taraska, 2017). In platelets, partial inhibition of PKC restores dense granules secretion (Unsworth et al., 2011). While our model assumes that the main consequence of increased exocytosis in the *pkcA*$^-$ line is to accentuate the starvation conditions, it is also possible that the vesicles carry out excess polyP into the medium (Fig. 8A,B).

The role of *pkcA* in cell proliferation in shear stress conditions

One of our most intriguing results was that *pkcA* was only important when cultures were grown under shaking conditions, in which *Dictyostelium* cells experience considerable shear stress (Taira and Yumura, 2017). Although it is unclear what relevance this might have in the natural history of this organism, our results should be of interest to cancer researchers. If a tumor is to become truly metastatic, any of the cells that will enter the blood or lymph must complete the epithelial-to-mesenchymal transition (EMT), part of which involves the cell switching to a non-proliferative mode. This is more appropriate during the migration phase, and will itself be reversed (in the mesenchymal-to-epithelial transition) if the migratory cell ever finds a suitable site to restart proliferation. The shear stress experienced during migration is critical for completion of the EMT (Liu et al., 2016; Xin et al., 2020). Also, previous studies in endothelial cells have shown that shear stress caused by blood flow induces PKC activation, and the association of PKC with F-actin (Hu and Chien, 1997). The *Dictyostelium* genome also has

many genes related to human cancer genes, which will be helpful in further studies of any interaction between them and *pkcA* (Kuspa et al., 2001; Eichinger et al., 2005). PKC-targeting drugs that have been considered for treating several types of cancer (Kim et al., 2008; Kreisl et al., 2010) may be more potent in high shear stress conditions, a point that deserves further study.

MATERIALS AND METHODS

Dictyostelium cell culture

The *D. discoideum* strains used in this study include: wild-type Ax2 (DBS0235534), NC4A2 (DBS034992), HPS400 (DBS023631), *pkcA*$^-$ (Mohamed et al., 2015), *i6kA*$^-$ (DBS0236426) (Luo et al., 2003), *ppk1*$^-$ (DBS0350686) (Zhang et al., 2007), *pldB*$^-$ (DBS0236796) (Chen et al., 2005), *abpA*$^-$/*C*$^-$ (DBS0235456) (Rivero et al., 1999), *lvsB*$^-$ (DBS0236521) (Harris et al., 2002), *proA*$^-$/*proB*$^-$ (DBS0236827) (Temesvari et al., 2000) and *scar*$^-$ (DBS0236924) (Seastone et al., 2001). The proliferation kinetics of all the parental Ax2 strains, DBS0235534 (*pkcA*$^-$, *abpA*$^-$/*C*$^-$ and *proA*$^-$/*B*$^-$), DBS0238015 (*ppk1*$^-$), DBS0235522 (*pldB*$^-$) and DBS0350762 (*i6kA*$^-$) used to generate the mutants were analyzed and found to be highly similar (Fig. S1A). The cells were grown axenically in shaking cultures or Petri dishes in maltose-HL5 medium (28.4 g bacteriological peptone, 15 g yeast extract, 18 g maltose monohydrate, 0.641 g Na_2HPO_4 and 0.49 g KH_2PO_4 per liter, pH 6.4) or minimal medium FM (Formedium, Norfolk, UK). Alternatively, *Dictyostelium* cells were also grown in SM/5 agar plates (2 g glucose, 2 g protease peptone, 0.4 g yeast extract, 1 g $MgSO_4{\cdot}7H_2O$, 0.66 g K_2HPO_4, 2.225 g KH_2PO_4 and 1.5 g bacto agar per litre, pH 6.4) in association with *K. aerogenes* at 22°C. *Scar*$^-$ and HPS400 cells were grown in HL5 supplemented with 100 µg/ml thymidine. The mutant strains carrying the antibiotic resistant markers were grown with either blasticidin (10 µg/ml) or G418 (20 µg/ml) (MP Biomedicals, USA). The fine chemicals, antibiotics and salts were obtained from Sigma-Aldrich, USA, MP Biomedicals, USA or Thermo Fisher Scientific, USA.

Generation of plasmid vectors and overexpressing strains

To generate the PkcA–GFP construct, the full-length *pkcA* gene (4044 bp) was PCR amplified from the genomic DNA and cloned into the pDM317 vector (Veltman et al., 2009) with GFP at the N-terminus. This gene cassette was cloned between BglII sites such that it was driven by a constitutive actin15 promoter. A 918 bp fragment encoding the catalytic domain of *pkcA* was PCR amplified and cloned in the pTX-GFP (Dicty Stock Center, USA; N-terminal GFP) vector by exploiting BamHI and XhoI restriction sites. For cloning the C1 domain (pkcA-C1-RFP), a 162 bp coding sequence was PCR amplified and engineered in the pTX-RFPmars (N-terminal RFP) vector (Fischer et al., 2004), between BamHI and XhoI restriction sites. For all PCR reactions, Expand PCR High Fidelity System (Roche, Indianapolis, USA) was used as per the manufacturer's protocols. Ax2 and *pkcA*$^-$ cells were independently transformed with pkcA–GFP, pkcA-cat–GFP and pkcA-C1–RFP constructs and the positive clones were selected with G418 (20 µg/ml).

Transformation by electroporation

Plasmid vectors were transformed into the cells by electroporation using a BTX ECM830 electroporator (Harvard Apparatus, USA). The cell suspension in HL5 medium was incubated at 22°C for 24 h, after which the cells were supplemented with 20 µg/ml G418 (MP Biomedicals, India) and were screened for G418-resistant clones. Subsequent to transformation, the clones were grown in HL5 medium supplemented with 10 µg/ml blasticidin (for selecting *pkcA*$^-$ cells) and 20 µg/ml G418 (all other strains).

Dictyostelium cells overexpressing PkcA (*pkcA*-OE) (Mohamed et al., 2015), coroninA (*corA*-OE) (Shina et al., 2011) and polyQ-containing exon 1 of human huntingtin with 103 consecutive glutamine residues (Q103–GFP; for the protein aggregation assay) (Malinovska et al., 2015) were grown in HL5 supplemented with 20 µg/ml G418. Ax2/*corA*-OE, *pkcA*$^-$/*corA*-OE, Ax2/Q103–GFP and *pkcA*$^-$/Q103–GFP cells were generated by transforming Ax2 and *pkcA*$^-$ cells by electroporating the *corA*-OE construct (Shina et al., 2011) (a kind gift from Dr Annette Müller-Taubenberger, LMU, Germany) and the Q103–GFP construct (Malinovska et al., 2015) (a kind gift from Dr Simon Alberti, MPI-CBG, Germany).

Cell proliferation assay

ML cells were resuspended in HL5 medium at a density of $1{\times}10^5$ cells/ml and kept in a shaker again at 150 rpm. For the proliferation assay in FM medium, cells were resuspended at $1{\times}10^6$ cells/ml. Every day, the cell density was determined using a hemocytometer. For the proliferation assay in Petri dishes, the ML cells were diluted to $1{\times}10^4$ cells/ml in Petri dishes containing 10 ml HL5. For the proliferation assay on a bacterial lawn, approximately 1000 *Dictyostelium* cells were mixed with 200 µl *Klebsiella aerogenes* and spread on three 90 mm Petri dishes in SM/5 medium. At the indicated time points, one of the plates was washed and the cells were counted using a hemocytometer. For all the conditions, the cells were incubated at 22°C.

Inhibitor treatment

Growth assays after drug treatments were performed as described in the figure legends. ML cells grown in HL5 suspension cultures were tested with 1, 3, 5, 10, 20 and 40 µM bisindolylmaleimide GF109203X (Bis I) (Mohamed et al., 2015; Toullec et al., 1991) (Sigma-Aldrich, USA) and the minimum effective inhibitory dose was found to be 5 µM.

Assay for PKC activity

The PKC activity was measured from ML and SP cell lysates as per the manufacturer's protocol (V5330, Promega, USA). *Dictyostelium* cells harvested from HL5 medium were adjusted to a density of $1{\times}10^8$ cells/ml in KK2 buffer, lysed in 500 µl–1 ml of PKC extraction buffer [25 mM Tris-HCl pH 7.4, 0.5 mM EDTA, 0.5 mM EGTA, 0.05% Triton X-100, 10 mM β-mercaptoethanol, 1× protease inhibitor cocktail (Sigma-Aldrich, USA) and 1× phosphatase inhibitor (Sigma-Aldrich, USA)]. A total of 9 µl of cell lysate was mixed with the PKC reaction mix containing PepTag C1 peptide and incubated at 30°C. After 30 min, the reaction was stopped by heating the samples at 95°C for 10 min. Then, 1 µl of 80% glycerol was added, the samples were run on a 0.8% agarose gel and were imaged. The kit uses a colored, fluorescent peptide substrate that is specific for PKC. Phosphorylation by PKC (cell lysates) alters the net charge of the peptide substrate, which allows the phosphorylated and un-phosphorylated versions of peptide substrate to rapidly separate on a agarose gel. The fluorescence intensity of phosphorylated peptide (a measure of PKC activity), was measured from the cell lysates using ImageJ (NIH, USA). The phosphorylated bands were analyzed and the intensity of each band was normalized to the total protein content. Total protein levels were assayed using Bradford reagent.

To determine the PKC activity in CM, at the indicated time points, the cell suspension was centrifuged (500 ***g*** for 7 min), the supernatant was concentrated 10-fold using 10 kDa cutoff filters (Amicon Ultracel-10K; Sigma-Aldrich, USA). 9 µl of concentrated CM was mixed with the PKC reaction mix for the PKC assay, which was performed as mentioned above.

Quantitative real-time PCR

Ax2 and *pkcA*$^-$ cells at ML and SP were harvested and RNA was extracted using FavorPrep™ Tri-RNA Reagent (Favorgen, Taiwan) (Pilcher et al., 2007). 1 µg of total RNA was used to synthesize cDNA using a cDNA synthesis kit as per manufacturer's protocol (Verso, Thermo Scientific, USA). Quantitative real-time PCR (qRT-PCR) was carried out with 1 µl of cDNA using DyNAmo Flash SYBR Green qPCR kit (Thermo Scientific, USA) to analyze the expression levels of *pkcA* (FW, 5′-TAA-TATGTCTCGGTCCACCA-3′ and REV, 5′-ATCAACTCTCATCACATC-GAC) and *i6kA* (FW, 5′-AAGCAATAGTGGTAACTTTAGCGG-3′ and REV, 5′-CAAATAGCCATCATCTTCTTGAGC-3′) using the Applied Biosystems® QuantStudio Flex 7 (Thermo Fisher Scientific, USA). *Ig7* (FW, 5′-TCCAAGAGGAAGAGGAGAACTGC-3′ and REV, 5′-TGG-GGAGGTCGTTACACCATTC-3′) was used as an mRNA amplification control. Real-time data was analyzed as described previoulsy (Schmittgen and Livak, 2008).

Journal of Cell Science (2022) 135, jcs259289. doi:10.1242/jcs.259289

Proliferation inhibition assay

The proliferation inhibition by CM was assayed by incubating the cells in 50% CM and 50% HL5 for 24 h at 22°C in non-shaking/shaking conditions (Suess and Gomer, 2016). The CM was harvested as mentioned in the figure legends. Cells grown in HL5 were considered as the control.

Polyphosphate measurements

CM preparation and polyP quantification were carried out as described previously (Suess and Gomer, 2016) with slight modifications. For fluorimetric measurements of extracellular polyP, cells were grown in FM medium to reduce the background fluorescence of HL5 medium (Franke and Kessin, 1977; Suess and Gomer, 2016). The CM was clarified by passing it through a 0.22 µm PVDF syringe filter, and the polyP levels were measured by staining the samples with 25 µg/ml DAPI for 5 min. Fluorescence intensity was measured at 415 nm excitation and 550 nm emission (Aschar-Sobbi et al., 2008) using a spectrofluorometer (Molecular Devices, USA). The polyP concentrations were obtained by using standards (kindly provided by Dr Toshikazu Shiba, RegeneTiss Inc., Japan). Intracellular polyP was extracted following the previously described protocol (Suess and Gomer, 2016) and was analyzed on a 25–30% polyacrylamide gel.

PAGE analysis of polyphosphates

PolyP levels were analyzed on polyacrylamide gels as previously described (Pisani et al., 2014) with the following modifications. ML- and SP-CM were purified through Midiprep columns (Qiagen Midiprep kit, Germany) (Desfougères et al., 2016). The polyP was eluted with the buffer provided by the manufacturer and polyP standards were run for reference. The gel images were quantified using ImageJ (NIH, USA).

Exopolyphosphatase treatment

The plasmid vector encoding the yeast recombinant exopolyphosphatase protein ScPPX1 was provided by Dr Michael Gray (University of Michigan, USA) (Gray et al., 2014). The CM was incubated with recombinant ScPPX1 at a concentration of 0.15 µg/ml along with 5 mM $MgCl_2$. Using 0.22 µm filters, the CM was filter sterilized and used directly as mentioned above. For the proliferation assay with ScPPX1, ML cells were inoculated at 1×10^5 cells/ml and 0.15 µg/ml ScPPX1 or buffer was added daily to cell culture during growth.

Western blotting

To examine the extracellular levels of AprA and CfaD, equal volumes of ML- and SP-CM were boiled with 6× SDS gel loading buffer at 100°C for 5 min. The protein samples were separated in a 12% SDS-polyacrylamide gel (Laemmli, 1970) and a parallel gel was run for silver staining. For measuring intracellular AprA and CfaD levels, cells were resuspended in lysis buffer [62.5 mM Tris-HCl pH 6.8, 2% SDS, 0.1 M DTT and 10% (v/v) glycerol] and boiled for 5 min. An equal concentration of protein was loaded on a 12% SDS-polyacrylamide gel and another gel was run for Coomassie staining. After electrophoresis, the proteins were transferred to a nitrocellulose membrane (BioRad, Laboratories, USA) and immunoblotted with anti-AprA (1:3000; Brock and Gomer, 2005) or anti-CfaD (1:1500; Bakthavatsalam et al., 2008) primary antibodies (a kind gift from Dr Richard Gomer, Texas A&M University, USA). After incubation with HRP-conjugated secondary antibody (1:5000; Bangalore Genei, India), the membrane was then treated with Clarity Western ECL substrate (BioRad Laboratories, USA) and the chemiluminescent signals were captured using ChemiDoc imaging systems (BioRad Laboratories, USA). The images were quantified using ImageJ (NIH, USA). Full images of gels used to quantify F-actin and myosin levels are given in Fig. S9.

Anti-AprA antibody treatment

To deplete extracellular AprA, the CM was treated with the anti-AprA antibody in a ratio of 1:150 for 2 h in 22°C. Subsequently, the proliferation inhibition assay was performed using the treated CM.

Fluid-phase pinocytosis and exocytosis assays

Fluid-phase endocytosis and exocytosis assays were carried out as described previously (Rivero and Maniak, 2006) with slight modifications. Log phase cells were harvested and resuspended at a concentration of 5×10^6 cells/ml in fresh HL5 medium and incubated for 15 min at 22°C at 150 rpm and then FITC–dextran (70,000 M_r; Sigma-Aldrich, USA) was added to a final concentration of 2 mg/ml. In the first 2 h, endocytosis of FITC–dextran was monitored by collecting the samples at indicated time points. After 2 h, cells were harvested, washed twice and resuspended in fresh HL5 medium. Exocytosis of FITC–dextran was monitored for the next 2 h. At the indicated time points, 500 µl of the cell sample was drawn and added to a tube containing 1.5 ml Sörensen's buffer (16.7 mM Na_2HPO_4/KH_2PO_4, pH 6.0), centrifuged (500 ***g*** for 3 min), washed twice with Sörensen's buffer, once with wash buffer (5 mM glycine, 100 mM sucrose, pH 8.5) and then stored on ice. The cells were lysed using 1 ml of lysis buffer containing 0.2% (v/v) Triton X-100. The fluorescence was measured at 492 nm excitation/525 nm emission; the intensity of fluorescence is a measure of the FITC–dextran level within the cells.

Endosomal pH assays

Endosomal pH was determined by the dual excitation ratio method as described previously (Rivero and Maniak, 2006) with slight modification. Briefly, ML cells were harvested and resuspended at a concentration of 3×10^6 cells/ml in HL5 medium containing FITC–dextran (2 mg/ml). After a 10 min pulse, cells were harvested and resuspended in HL5 medium without FITC–dextran. At 10 min intervals, 500 µl of cells was collected and added to a tube containing ice-cold MES buffer (50 mM), washed twice and then resuspended in 1 ml MES. The fluorescence intensity was measured after dual excitation at 450 nm and 495 nm, and emission at 525 nm. The fluorescence ratio (value after excitation at 495 nm/value after excitation at 450 nm) was calculated and the endosomal pH was obtained by comparing to a standard curve. To obtain the standard curve for pH, the fluorescence of FITC–dextran in various pH conditions (pH 4–7) was measured.

F-actin staining

ML cells were harvested, seeded onto coverslips with HL5 and incubated at 22°C for 2 h. The cells were then washed with KK2 buffer, fixed with 3.7% formaldehyde in phosphate-buffered saline (PBS) for 10 min, washed with PBS, permeabilized with 0.5% Triton-X 100 in PBS and washed with PBS again. To visualize F-actin, the cells were stained with 300 nM TRITC–phalloidin (Sigma-Aldrich, USA) for 1 h in dark conditions. The samples were washed with PBS and mounted on a slide with AntiFade Gold (ThermoFisher Scientific, USA) mounting solution. The images were taken with an Olympus FV 3000 confocal microscope using a 63× objective lens and the images were processed with ImageJ software (NIH, USA).

F-actin and myosin polymerization assays

The cytoskeletal proteins were isolated as detergent-insoluble fractions using a NP-40 lysis buffer (Chung and Firtel, 1999). ML cells were harvested from HL5 medium, resuspended at 10^8 cells/ml and lysed with 2× lysis buffer (50 mM Tris-HCl pH 7.6, at room temperature, 200 mM NaCl, 20 mM NaF, 2 mM sodium vanadate, 6 mM sodium pyrophosphate, 2 mM EDTA, 2 mM EGTA, 1× protease inhibitor cocktail, 2% NP-40, 20% glycerol, 2 mM DTT). The lysed samples were vortexed, placed on ice for 10 min, then kept at room temperature for 10 min. The samples were then spun for 4 min at 11,000 ***g*** and the collected pellet was washed twice with 1× lysis buffer, and dissolved in 2× SDS gel loading buffer by boiling at 100°C for 10 min. The samples were run on a 12% gel (for F-actin) or a 8% gel (for myosin). The protein bands were stained with Coomassie Blue R250, scanned and changes in F-actin and myosin levels were measured densitometrically, using ImageJ (NIH, USA).

To check myosin function (Tuxworth et al., 1997), axenically grown cells were harvested and resuspended in KK2 buffer, seeded onto six-well plates and allowed to settle. The buffer was replaced with 0.01% sodium azide in KK2 and incubated for 30 min. The fraction of detached and adhered cells was counted after 30 min.

Traction-mediated cytofission assays

PkcA^{-} cells were grown for 5 days in shaking conditions and an aliquot was transferred to the coverslips. The cells were allowed to settle and, once the cells showed cytofission, they were fixed, stained and imaged as described above (Tuxworth et al., 1997).

Estimating DNA content

The DNA content was determined by fixing ML cells with ice cold methanol for 20 min in −20°C. The fixed cells were placed on a glass slide using DAPI-containing mounting solution (Sigma-Aldrich, USA), imaged on a Nikon Eclipse 80i upright microscope (Nikon, Japan) and analyzed using ImageJ (NIH, USA).

Propidium iodide staining and flow cytometry for cell cycle analysis

Flow cytometry was carried out to examine cell size and cell cycle as previously described (Chen and Kuspa, 2005). *Dictyostelium* cells were grown in HL5 medium at 22°C in Petri dishes or with constant shaking (150 rpm). Cells were harvested, washed twice and 1×10^7 cells were resuspended in KK2 buffer. Then, the cells were fixed with 3 ml 70% ice-cold ethanol and incubated for 30 min at −20°C. Fixed cells were pelleted and resuspended in 1 ml of propidium iodide (PI; Sigma-Aldrich, USA; 10 µg/ml in KK2 buffer). Then, 1 µl of 100 mg/ml DNase-free RNase (Sigma-Aldrich, USA) was added and cells were incubated at 37°C. Flow cytometry was carried out with a CytoFLEX apparatus (Beckman-Coulter, USA). Cell size was determined by forward scatter and cell cycle was analyzed by measuring the fraction of PI stained population. At least 10,000 cells were counted for each analysis and were sampled in biological triplicates.

Colocalization studies of PkcA–GFP with subcellular markers

To identify the subcellular organelles where PkcA–GFP was localized, we used 3 µM Acridine Orange (AO) (Sigma-Aldrich) marking acidic vesicles (Padh et al., 1989), or 200 nM LysoTracker RED (Thermo Fisher Scientific) marking lysosomes (Li et al., 2016) or 5 µM MitoTracker RED (Thermo Fisher Scientific) marking mitochondria (Schimmel et al., 2012). Endosomal vesicles were marked by either FITC–dextran (2 mg/ml) or TRITC–dextran (2 mg/ml). To test the effect of F-actin polymerization on PkcA–GFP localization, 10 µM latrunculin B (Kriebel et al., 2008) (Sigma-Aldrich) was used. To test the effect of PKC activity on PkcA–GFP localization, 10 µM Bis I was used on the cells. The cells were imaged using a Zeiss laser scanning LSM 710 confocal microscope. Imaging was carried out using a pinhole of 1 Airy unit, or, for MitoTracker, a pinhole of 1.36 Airy units (Schimmel et al., 2012).

Protein aggregation assay

Dictyostelium cells containing Q103–GFP (polyQ-containing exon 1 of human huntingtin with 103 consecutive glutamines) vector were harvested from ML and at SP, seeded onto coverslips with HL5 and incubated at 22°C for 30 min. Thereafter, the cells were washed with KK2 buffer and fixed in 3.7% formaldehyde in phosphate-buffered saline (PBS) for 10 min, and washed with PBS. The samples were observed using the 63× objective lens of a confocal microscope Nikon A1 HD. *Z*-stacks of 20 slices were taken and the maximum intensity was projected using the slices. The RGB images were converted to 8-bit images and then analyzed for the presence of Q103–GFP protein aggregates. Q103–GFP protein aggregates form fluorescent foci in the cells. Cells with the foci were counted in each condition and percentage of cells containing the aggregate foci was calculated.

Statistical analysis

Data analysis was done using GraphPad Prism software (GraphPad Prism software, San Diego, CA). Statistical significance was assessed using a Student's *t*-test, or by ANOVA as indicated in the figure legends. Significance was defined as $P<0.05$.

Acknowledgements

We gratefully acknowledge the help of *Dictyostelium* Stock Center (Northwestern University, USA) for providing the strains and plasmids used in the study, Dr Richard Gomer for the anti-AprA and anti-CfaD antibodies, Dr Annette Müller-Taubenberger for the coronin A overexpression (*corA*-OE) plasmid, Dr Simon Alberti for the Q103-GFP plasmid, Dr Michael Gray for the ScPPX1 plasmid, Dr Toshikazu Shiba of RegeneTiss Inc for the polyP standards. We acknowledge the facilities, the scientific technical assistance of the Advanced Microscopy Facility at NCTB, Department of Biotechnology, IIT Madras. S.U. acknowledges the help of Rakesh Mani, Dr Nasna Nassir, Vignesh R., Prajna A. Rai and Pavani Hathi. We gratefully acknowledge Industrial Consultancy and Sponsored Research (ICSR) and IIT Madras for all the support.

Competing interests

The authors declare no competing or financial interests.

Author contributions

Conceptualization: S.U., R.B.; Methodology: S.U., W.M., M.J., R.B.; Software: S.U.; Validation: S.U., W.M., M.J., D.B., R.B.; Formal analysis: S.U., G.H., R.B.; Investigation: S.U., W.M., M.J.; Resources: S.U., G.H., R.B.; Data curation: S.U., W.M., R.B.; Writing - original draft: S.U.; Writing - review & editing: S.U., W.M., M.J., G.H., D.B., R.B.; Visualization: S.U., G.H., D.B., R.B.; Supervision: R.B.; Project administration: S.U., R.B.; Funding acquisition: R.B.

Funding

This research received no specific grant from any funding agency in the public, commercial or not-for-profit sectors.

References

Aschar-Sobbi, R., Abramov, A. Y., Diao, C., Kargacin, M. E., Kargacin, G. J., French, R. J. and Pavlov, E. (2008). High sensitivity, quantitative measurements of polyphosphate using a new DAPI-based approach. *J. Fluoresc.* **18**, 859-866. doi:10.1007/s10895-008-0315-4

Bakthavatsalam, D., Brock, D. A., Nikravan, N. N., Houston, K. D., Hatton, R. D. and Gomer, R. H. (2008). The secreted *Dictyostelium* protein CfaD is a chalone. *J. Cell Sci.* **121**, 2473-2480. doi:10.1242/jcs.026682

Brauer, M. J., Huttenhower, C., Airoldi, E. M., Rosenstein, R., Matese, J. C., Gresham, D., Boer, V. M., Troyanskaya, O. G. and Botstein, D. (2008). Coordination of growth rate, cell cycle, stress response and metabolic activity in yeast. *Mol. Biol. Cell* **19**, 352-367. doi:10.1091/mbc.e07-08-0779

Brock, D. A. and Gomer, R. H. (2005). A secreted factor represses cell proliferation in *Dictyostelium*. *Development* **132**, 4553-4562. doi:10.1242/dev.02032

Buratta, S., Tancini, B., Sagini, K., Delo, F., Chiaradia, E., Urbanelli, L. and Emiliani, C. (2020). Lysosomal exocytosis, exosome release and secretory autophagy: The autophagic- and endo-lysosomal systems go extracellular. *Int. J. Mol. Sci.* **21**, 2576. doi:10.3390/ijms21072576

Cazzanelli, G., Pereira, F., Alves, S., Francisco, R., Azevedo, L., Carvalho, P. D., Almeida, A., Côrte-Real, M., Oliveira, M., Lucas, C. et al. (2018). The yeast *Saccharomyces cerevisiae* as a model for understanding RAS proteins and their role in Human tumorigenesis. *Cells* **7**, 14. doi:10.3390/cells7020014

Charette, S. J. and Cosson, P. (2007). A LYST/beige homolog is involved in biogenesis of *Dictyostelium* secretory lysosomes. *J. Cell Sci.* **120**, 2338-2343. doi:10.1242/jcs.009001

Chen, G. and Kuspa, A. (2005). Prespore cell fate bias in G1 phase of the cell cycle in Dictyostelium discoideum. *Eukaryot. Cell* **4**, 1755-1764. doi:10.1128/EC.4.10.1755-1764.2005

Chen, Y., Rodrick, V., Yan, Y. and Brazil, D. (2005). PldB, a putative phospholipase D homologue in *Dictyostelium discoideum* mediates quorum sensing during development. *Eukaryot. Cell* **4**, 694-702. doi:10.1128/EC.4.4.694-702.2005

Chen, Z., Forman, L. W., Williams, R. M. and Faller, D. V. (2014). Protein kinase C-delta inactivation inhibits the proliferation and survival of cancer stem cells in culture and in vivo. *BMC Cancer* **14**, 90-105. doi:10.1186/1471-2407-14-90

Chopra, R., Wasserman, A. H., Pulst, S. M., De Zeeuw, C. I. and Shakkottai, V. G. (2018). Protein kinase C activity is a protective modifier of Purkinje neuron degeneration in cerebellar ataxia. *Hum. Mol. Genet.* **27**, 1396-1410. doi:10.1093/hmg/ddy050

Chung, C. Y. and Firtel, R. A. (1999). PAKa, a putative PAK family member, is required for cytokinesis and the regulation of the cytoskeleton in *Dictyostelium discoideum* cells during chemotaxis. *J. Cell Biol.* **147**, 559-575. doi:10.1083/jcb.147.3.559

Consalvo, K. M., Rijal, R., Tang, Y., Kirolos, S. A., Smith, M. R. and Gomer R. H. (2019). Extracellular signaling in *Dictyostelium*. *Int. J. Dev. Biol.* **63**, 395-405. doi:10.1387/ijdb.190259rg

De Araujo, M. E. G., Liebscher, G., Hess, M. W. and Huber, L. A. (2020). Lysosomal size matters. *Traffic* **21**, 60-75. doi:10.1111/tra.12714

Desfougères, Y., Gerasimaite, R., Jessen, H. J. and Mayer, A. (2016). Vtc5, a novel subunit of the vacuolar transporter chaperone complex, regulates

polyphosphate synthesis and phosphate homeostasis in yeast. *J. Biol. Chem.* **291**, 22262-22275. doi:10.1074/jbc.M116.746784

Eichinger, L., Pachebat, J. A., Glockner, G., Rajandream, M.-A., Sucgang, R., Berriman, M., Song, J., Olsen, R., Szafranski, K., Xu, Q. et al. (2005). The genome of the social amoeba *Dictyostelium discoideum*. *Nature* **435**, 43-57. doi:10.1038/nature03481

Fazzari, P., Horre, K., Arranz, A. M., Frigerio, C. S., Saito, T., Saido, T. C. and De Strooper, B. (2017). *PLD3* gene and processing of APP. *Nature* **541**, E1-E2. doi:10.1038/nature21030

Fischer, M., Haase, I., Simmeth, E., Gerisch, G. and Müller-Taubenberger, A. (2004). A brilliant monomeric red fluorescent protein to visualize cytoskeleton dynamics in *Dictyostelium*. *FEBS Lett.* **577**, 227-232. doi:10.1016/j.febslet.2004.09.084

Franke, J. and Kessin, R. (1977). A defined minimal medium for axenic strains of *Dictyostelium discoideum*. *Proc. Natl. Acad. Sci. USA* **74**, 2157-2161. doi:10.1073/pnas.74.5.2157

Fukumoto, S., Nishizawa, Y., Hosoi, M., Koyama, H., Yamakawa, K., Ohno, S. and Morii, H. (1997). Protein Kinase C δ inhibits the proliferation of vascular smooth muscle cells by suppressing G1 cyclin expression. *J. Biol. Chem.* **272**, 13816-13822. doi:10.1074/jbc.272.21.13816

Gaidenko, T. A., Kim, T.-J. and Price, C. W. (2002). The PrpC serine-threonine phosphatase and PrkC kinase have opposing physiological roles in stationary-phase *Bacillus subtilis* cells. *J. Bacteriol.* **184**, 6109-6114. doi:10.1128/JB.184.22.6109-6114.2002

Graham, M. A., Rawe, I., Dartt, D. A. and Joyce, N. C. (2000). Protein kinase C regulation of corneal endothelial cell proliferation and cell cycle. *Invest. Ophthalmol. Vis. Sci.* **41**, 4124-4132.

Gray, M. J., Wholey, W.-Y., Wagner, N. O., Cremers, C. M., Mueller-Schickert, A., Hock, N. T., Krieger, A. G., Smith, E. M., Bender, R. A., Bardwell, J. C. A. et al. (2014). Polyphosphate is a primordial chaperone. *Mol. Cell* **53**, 689-699. doi:10.1016/j.molcel.2014.01.012

Guaragnella, N., Palermo, V., Galli, A., Moro, L., Mazzoni, C. and Giannattasio, S. (2014). The expanding role of yeast in cancer research and diagnosis: insights into the function of the oncosuppressors p53 and BRCA1/2. *FEMS Yeast Res.* **14**, 2-16. doi:10.1111/1567-1364.12094

Harris, E., Wang, N., Wu, W.-L., Weatherford, A., Lozanne, A. D. and Cardelli, J. (2002). *Dictyostelium* LvsB mutants model the lysosomal defects associated with Chediak-Higashi syndrome. *Mol. Biol. Cell* **13**, 656-669. doi:10.1091/mbc.01-09-0454

Heinisch, J. J., Lorberg, A., Schmitz, H.-P. and Jacoby, J. J. (1999). The protein kinase C-mediated MAP kinase pathway involved in the maintenance of cellular integrity in *Saccharomyces cerevisiae*. *Mol. Microbiol.* **32**, 671-680. doi:10.1046/j.1365-2958.1999.01375.x

Herman, P. K. (2002). Stationary phase in yeast. *Curr. Opin. Microbiol.* **5**, 602-607. doi:10.1016/S1369-5274(02)00377-6

Hu, Y.-L. and Chien, S. (1997). Effects of shear stress on protein kinase C distribution in endothelial cells. *J. Histochem. Cytochem.* **45**, 237-249. doi:10.1177/002215549704500209

Jackson, M. P. and Hewitt, E. W. (2016). Cellular proteostasis: degradation of misfolded proteins by lysosomes. *Essays Biochem.* **60**, 173-180. doi:10.1042/EBC20160005

Jiang, M., Shao, W., Perego, M. and Hoch, J. A. (2000). Multiple histidine kinases regulate entry into stationary phase and sporulation in *Bacillus subtillis*. *Mol. Microbiol.* **38**, 535-542. doi:10.1046/j.1365-2958.2000.02148.x

Kang, J.-H. (2014). Protein Kinase C (PKC) isozymes and cancer. *New J. Sci.* **2014**, 1-36. doi:10.1155/2014/231418

Kim, J., Choi, Y.-L., Vallentin, A., Hunrichs, B. S., Hellerstein, M. K., Peehl, D. M. and Mochly-Rosen, D. (2008). Centrosomal PKCβII and pericentrin are critical for Human prostate cancer growth and angiogenesis. *Cancer Res.* **68**, 6831-6839. doi:10.1158/0008-5472.CAN-07-6195

Krause, S. A. and Gray, J. V. (2002). The protein kinase C pathway is required for viability in quiescence in *Saccharomyces cerevisiae*. *Curr. Biol.* **12**, 588-593. doi:10.1016/S0960-9822(02)00760-1

Kreisl, T. N., Kotliarova, S., Butman, J. A., Albert, P. S., Kim, L., Musib, L., Thornton, D. and Fine, H. A. (2010). A phase I/II trial of enzastaurin in patients with recurrent high-grade gliomas. *Neuro-Oncol.* **12**, 181-189. doi:10.1093/neuonc/nop042

Kriebel, P. W., Barr, V. A., Rericha, E. C., Zhang, G. and Parent, C. A. (2008). Collective cell migration requires vesicular trafficking for chemoattractant delivery at the trailing edge. *J. Cell Biol.* **183**, 949-961. doi:10.1083/jcb.200808105

Kuspa, A., Sucgang, R. and Shaulsky, G. (2001). The promise of a protist: the *Dictyostelium* genome project. *Funct. Integr. Genomics* **1**, 279-293. doi:10.1007/s101420000033

Laemmli, U. K. (1970). Cleavage of structural proteins during the assembly of the head of bacteriophage T4. *Nature* **227**, 680-685. doi:10.1038/227680a0

Li, Y., Xu, M., Ding, X., Yan, C., Song, Z., Chen, L., Huang, X., Wang, X., Jian, Y., Tang, G. et al. (2016). Protein kinase C controls lysosome biogenesis independently of mTORC1. *Nat. Cell Biol.* **18**, 1065-1077. doi:10.1038/ncb3407

Liu, S., Zhou, F., Shen, Y., Zhang, Y., Yin, H., Zeng, Y., Liu, J., Yan, Z. and Liu, X. (2016). Fluid shear stress induces epithelial-mesenchymal transition (EMT) in Hep-2 cells. *Oncotarget* **7**, 32876-32892. doi:10.18632/oncotarget.8765

Luo, H. R., Huang, Y. E., Chen, J. C., Saiardi, A., Iijima, M., Ye, K., Huang, Y., Nagata, E., Devreotes, P. and Snyder, S. H. (2003). Inositol pyrophosphates mediate chemotaxis in *Dictyostelium* via Pleckstrin homology Domain-PtdIns(3,4,5)P3 interactions. *Cell* **114**, 559-572. doi:10.1016/S0092-8674(03)00640-8

Malinovska, L., Palm, S., Gibson, K., Verbavatz, J.-M. and Alberti, S. (2015). *Dictyostelium discoideum* has a highly Q/N-rich proteome and shows an unusual resilience to protein aggregation. *Proc. Natl. Acad. Sci. USA* **112**, E2620-E2629. doi:10.1073/pnas.1504459112

Matuo, R., Sousa, F. G., Soares, D. G., Bonatto, D., Saffi, J., Escargueil, A. E., Larsen, A. K. and Henriques, J. A. P. (2012). *Saccharomyces cerevisiae* as a model system to study the response to anticancer agents. *Cancer Chemother. Pharmacol.* **70**, 491-502. doi:10.1007/s00280-012-1937-4

Mohamed, W., Ray, S., Brazill, D. and Baskar, R. (2015). Absence of catalytic domain in a putative protein kinase C (PkcA) suppresses tip dominance in *Dictyostelium discoideum*. *Dev. Biol.* **405**, 10-20. doi:10.1016/j.ydbio.2015.05.021

Musashi, M., Ota, S. and Shiroshita, N. (2000). The role of protein kinase C isoforms in cell proliferation and apoptosis. *Int. J. Hematol.* **72**, 12-19.

Nanos-Webb, A., Bui, T., Karakas, C., Zhang, D., Carey, J. P. W., Mills, G. B., Hunt, K. K. and Keyomarsi, K. (2016). PKC iota promotes ovarian tumor progression through deregulation of cyclin E. *Oncogene* **35**, 2428-2440. doi:10.1038/onc.2015.301

Neuhaus, E. M., Almers, W. and Soldati, T. (2002). Morphology and dynamics of the endocytic pathway in *Dictyostelium discoideum*. *Mol. Biol. Cell* **13**, 1390-1407. doi:10.1091/mbc.01-08-0392

Padh, H., Lavasa, M. and Steck, T. L. (1989). Prelysosomal acidic vacuoles in *Dictyostelium discoideum*. *J. Cell Biol.* **108**, 865-874. doi:10.1083/jcb.108.3.865

Parish, R. W. and Weibel, M. (1980). Extracellular ATP, ecto-ATPase and calcium influx in *Dictyostelium discoideum* cells. *FEBS Lett.* **118**, 263-266. doi:10.1016/0014-5793(80)80234-1

Pilcher, K. E., Gaudet, P., Fey, P., Kowal, A. S. and Chisholm, R. L. (2007). A general purpose method for extracting RNA from *Dictyostelium* cells. *Nat. Protoc.* **2**, 1329-1332. doi:10.1038/nprot.2007.191

Pisani, F., Livermore, T., Rose, G., Chubb, J. R., Gaspari, M. and Saiardi, A. (2014). Analysis of *Dictyostelium discoideum* inositol pyrophosphate metabolism by gel electrophoresis. *PLoS ONE* **9**, e85533. doi:10.1371/journal.pone.0085533

Reinders, A., Burckert, N., Boller, T., Wiemken, A. and De Virgilio, C. (1998). *Saccharomyces cerevisiae* cAMP-dependent protein kinase controls entry into stationary phase through the Rim15p protein kinase. *Genes Dev.* **12**, 2943-2955. doi:10.1101/gad.12.18.2943

Rivero, F. (2008). Endocytosis and the actin cytoskeleton in *Dictyostelium discoideum*. *Int. Rev. Cell Mol. Biol.* **267**, 343-397. doi:10.1016/S1937-6448(08)00633-3

Rivero, F. and Maniak, M. (2006). Quantitative and microscopic methods for studying and endocytic patway. In *Methods in Molecular Biology: Dictostelium discoideum Protocols* (ed. L. Eichinger and F. Rivero), pp. 423-438. Totowa, NJ: Humana Press Inc.

Rivero, F., Furukawa, R., Fechheimer, M. and Noegel, A. A. (1999). Three actin cross-linking proteins, the 34 kDa actin-bundling protein, α-actinin and gelation factor (ABP-120), have both unique and redundant roles in the growth and development of *Dictyostelium*. *J. Cell Sci.* **112**, 2737-2751. doi:10.1242/jcs.112.16.2737

Rose, A. J., Michell, B. J., Kemp, B. E. and Hargreaves, M. (2004). Effect of exercise on protein kinase C activity and localization in human skeletal muscle. *J. Physiol.* **561**, 861-870. doi:10.1113/jphysiol.2004.075549

Santarriaga, S., Petersen, A., Ndukwe, K., Brandt, A., Gerges, N., Scaglione, J. B. and Scaglione, K. M. (2015). The social amoeba *Dictyostelium discoideum* is highly resistant to polyglutamine aggregation. *J. Biol. Chem.* **290**, 25571-25578. doi:10.1074/jbc.M115.676247

Schimmel, B. G., Berbusse, G. W. and Naylor, K. (2012). Mitochondrial fission and fusion in *Dictyostelium discoideum*: a search for proteins involved in membrane dynamics. *BMC Res. notes* **5**, 505. doi:10.1186/1756-0500-5-505

Schmittgen, T. D. and Livak, K. J. (2008). Analyzing real-time PCR data by the comparative C(T) method. *Nat. Protoc.* **3**, 1101-1108. doi:10.1038/nprot.2008.73

Seastone, D. J., Harris, E., Temesvari, L. A., Bear, J. E., Saxe, C. L. and Cardelli, J. (2001). The WASp-like protein Scar regulates macropinocytosis, phagocytosis and endosomal membrane flow in *Dictyostelium*. *J. Cell Sci.* **114**, 2673-2683. doi:10.1242/jcs.114.14.2673

Shina, M. C., Müller-Taubenberger, A., Ünal, C., Schleicher, M., Steinert, M., Eichinger, L., Muller, R., Blau-Wasser, R., Glöckner, G. and Noegel, A. A. (2011). Redundant and unique roles of coronin proteins in *Dictyostelium*. *Cell. Mol. Life Sci.* **68**, 303-313. doi:10.1007/s00018-010-0455-y

Singh, S., Mohamed, W., Aguessy, A., Dyett, E., Shah, S., Khan, M., Baskar, R. and Brazill, D. (2017). Functional interaction of PkcA and PldB regulate aggregation and development in *Dictyostelium discoideum*. *Cell. Signal.* **34**, 47-54. doi:10.1016/j.cellsig.2017.02.022

Sivaramakrishnan, V. and Fountain, S. J. (2015). Evidence for extracellular ATP as a stress signal in a single-celled organism. *Eukaryot. Cell* **14**, 775-782. doi:10.1128/EC.00066-15
Soll, D. R., Yarger, J. and Mirick, M. (1976). Stationary phase and the cell cycle of *Dictyostelium discoideum* in liquid nutrient medium. *J. Cell Sci.* **20**, 513-523. doi:10.1242/jcs.20.3.513
Steinberg, S. F. (2008). Structural basis of protein kinase C isoform function. *Physiol. Rev.* **88**, 1341-1378. doi:10.1152/physrev.00034.2007
Suess, P. M. and Gomer, R. H. (2016). Extracellular polyphosphate inhibits proliferation in an autocrine negative feedback loop in *Dictyostelium discoideum*. *J. Biol. Chem.* **291**, 20260-20269. doi:10.1074/jbc.M116.737825
Suess, P. M., Watson, J., Chen, W. and Gomer, R. H. (2017). Extracellular polyphosphate signals through Ras and Akt to prime *Dictyostelium discoideum* cells for development. *J. Cell Sci.* **130**, 2394-2404. doi:10.1242/jcs.203372
Suess, P. M., Tang, Y. and Gomer, R. H. (2019). The putative G protein–coupled receptor GrlD mediates extracellular polyphosphate sensing in *Dictyostelium discoideum*. *Mol. Biol. cell.* **30**, 1118-1128. doi:10.1091/mbc.E18-10-0686
Taira, R. and Yumura, S. (2017). A novel mode of cytokinesis without cell-substratum adhesion. *Sci. Rep.* **7**, 17694. doi:10.1038/s41598-017-17477-w
Tancini, B., Buratta, S., Delo, F., Sagini, K., Chiaradia, E., Pellegrino, R. M., Emiliani, C. and Urbanelli, L. (2020). Lysosomal exocytosis: the extracellular role of an intracellular organelle. *Membranes* **10**, 406. doi:10.3390/membranes10120406
Tang, Y., Rijal, R., Zimmerhanzel, D. E., McCullough, J. R., Cadena, L. A., Gomer, R. H. and Heitman, J. (2021). An autocrine negative feedback loop inhibits *Dictyostelium discoideum* proliferation through pathways including IP3/Ca^{2+}. *mBio* **12**, e01347-e01321. doi:10.1128/mBio.01347-21
Temesvari, L., Schleicher, M., Zhang, L., Fodera, B., Janssen, K.-P. and Cardelli, J. A. (2000). Inactivation of lmpA, encoding a LIMPII-related endosomal protein, suppresses the internalization and endosomal trafficking defects in profilin-null mutants. *Mol. Biol. Cell* **11**, 2019-2031. doi:10.1091/mbc.11.6.2019
Toullec, D., Pianetti, P., Coste, H., Bellevergue, P., Grand-Perret, T., Ajakane, M., Baudet, V., Boissin, P., Boursier, E., Loriolle, F. et al. (1991). The Bisindolylmaleimide GF 109203X is a potent and selective inhibitor of protein kinase C. *J. Biol. Chem.* **266**, 15771-15781. doi:10.1016/S0021-9258(18)98476-0
Trexler, A. J. and Taraska, J. W. (2017). Regulation of insulin exocytosis by calcium-dependent protein kinase C in beta cells. *Cell Calcium* **67**, 1-10. doi:10.1016/j.ceca.2017.07.008
Tuxworth, R. I., Cheetham, J. L., Machesky, L. M., Spiegelmann, G. B., Weeks, G. and Insall, R. H. (1997). *Dictyostelium* RasG is required for normal motility and cytokinesis, but not growth. *J. Cell Biol.* **138**, 605-614. doi:10.1083/jcb.138.3.605
Unsworth, A. J., Smith, H., Gissen, P., Watson, S. P. and Pears, C. J. (2011). Submaximal inhibition of protein kinase C restores ADP-induced dense granule secretion in platelets in the presence of Ca2+. *J. Biol. Chem.* **286**, 21073-21082. doi:10.1074/jbc.M110.187138
Veltman, D. M., Akar, G., Bosgraaf, L. and Van Haastert, P. J. M. (2009). A new set of small, extrachromosomal expression vectors for *Dictyostelium discoideum*. *Plasmid* **61**, 110-118. doi:10.1016/j.plasmid.2008.11.003
Veltman, D. M., Williams, T. D., Bloomfield, G., Chen, B.-C., Betzig, E., Insall, R. H. and Kay, R. R. (2016). A plasma membrane template for macropinocytic cups. *eLife* **5**, e20085. doi:10.7554/eLife.20085
Wang, P., Zhou, Z., Hu, A., Ponte de Albuquerque, C., Zhou, Y., Hong, L., Sierecki, E., Ajiro, M., Kruhlak, M., Harris, C. et al. (2014). Both decreased and increased SRPK1 levels promote cancer by interfering with PHLPP-mediated dephosphorylation of Akt. *Mol. Cell* **54**, 378-391. doi:10.1016/j.molcel.2014.03.007
Werner-Washburne, M., Brown, D. and Braun, E. (1991). Bcyl, the regulatory subunit of cAMP-dependent protein kinase in yeast, is differentially modified in response to the physiological status of the cell. *J. Biol. Chem.* **266**, 19704-19709. doi:10.1016/S0021-9258(18)55049-3
Wight, E. M., Ide, A. D. and Damer, C. K. (2020). Copine A regulates the size and exocytosis of contractile vacuoles and postlysosomes in *Dictyostelium*. *FEBS Open Bio* **10**, 979-994. doi:10.1002/2211-5463.12874
Xin, Y., Li, K., Yang, M. and Tan, Y. (2020). Fluid shear stress induces EMT of circulating tumor cells via JNK signaling in favor of their survival during hematogenous dissemination. *Int. J. Mol. Sci.* **21**, 8115. doi:10.3390/ijms21218115
Yang, Q., Zhang, X.-F., Van Goor, D., Dunn, A. P., Hyland, C., Medeiros, N. and Forscher, P. (2013). Protein kinase C activation decreases peripheral actin network density and increases central nonmuscle myosin II contractility in neuronal growth cones. *Mol. Biol. Cell* **24**, 3097-3114. doi:10.1091/mbc.e13-05-0289
Yarger, J., Stults, K. and Soll, D. R. (1974). Observations on the growth of *Dictyostelium discoideum* in axenic medium: Evidence for an extracellular growth inhibitor synthesized by stationary phase cells. *J. Cell Sci.* **14**, 681-690. doi:10.1242/jcs.14.3.681
Zhang, H., Gómez-Garcia, M. R., Shi, X., Rao, N. N. and Kornberg, A. (2007). Polyphosphate kinase 1, a conserved bacterial enzyme, in a eukaryote, *Dictyostelium discoideum*, with a role in cytokinesis. *Proc. Natl. Acad. Sci. USA* **104**, 16486-16491. doi:10.1073/pnas.0706847104

Fig. S1. Proliferation curves of *Dictyostelium* strains under growth conditions.

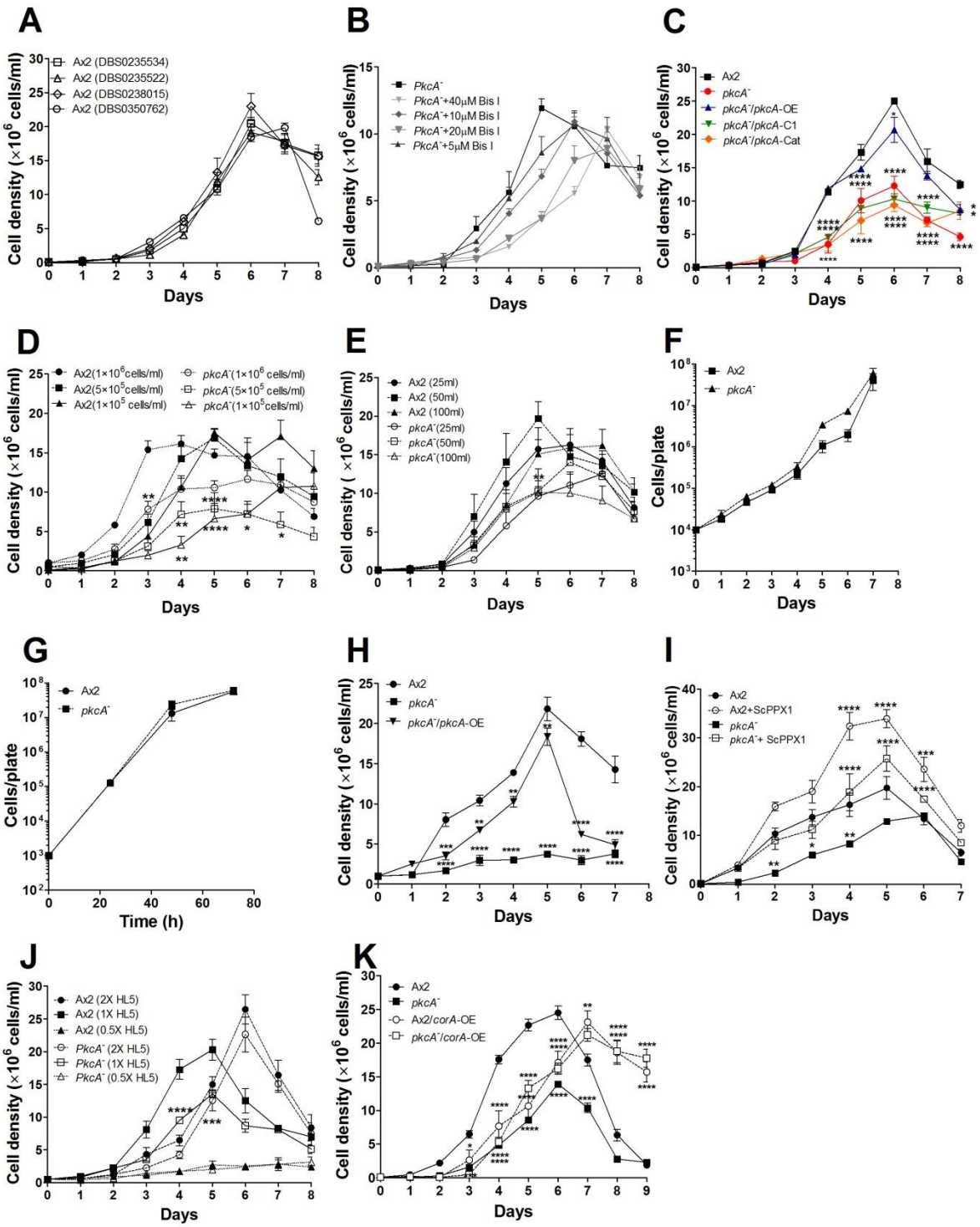

Fig. S1. Proliferation curves of *Dictyostelium* strains under growth conditions. (A) Proliferation assays of all the parental Ax2 strains used to generate various mutants used in the study. SP densities (in units of 10^6 cells/ml) were 21.3±0.4 for Ax2 (DBS0235534), 23.0±1.9 for Ax2 (DBS0238015), 19.9±0.8 for Ax2 (DBS0235522) and 20.4±0.7 for Ax2 (DBS0350762). (B) *PkcA*$^-$ cells were treated with different concentrations of Bis I at an interval of 24 h, and the proliferation assays were then carried out. The density at which cells enter SP was dependent on the Bis I dose ((10 μM ($p<0.05$), 20 μM ($p<0.01$) and 40 μM ($p<0.001$)(one- way ANOVA with Tukey's multiple comparisons)). (C) To determine the particular domain of pkcA that is important for cell proliferation and SP entry, *pkcA*$^-$ cells were independently transformed with the regulatory C1 (*pkcA*$^-$/act15::*pkcA*-C1domain) and the catalytic kinase domain (*pkcA*$^-$ /act15::*pkcA*-cat domain) and a proliferation assay with a starting density of 1×10^5 cells/ml was performed. The cell number was determined every day using a hemocytometer. SP cell density is included in Table S1. (D) Cells were inoculated at the indicated initial densities and proliferation assays were performed. The proliferation kinetics of *pkcA*$^-$ cells inoculated at 1×10^5, 5×10^5 and 1×10^6 cells/ml were compared to Ax2 cells at the respective density. (E) To check if differences in aeration affect cell proliferation, Ax2 and *pkcA*$^-$ cells were cultured in three different sized flasks (25, 50 and 100 ml with 10 ml media in each) and the cell density was determined using a hemocytometer every day. The proliferation curves of *pkcA*$^-$ cells grown in 25, 50 and 100 ml flasks were compared to those of Ax2 grown in 25, 50 and 100 ml flasks respectively. (F) Proliferation assay in Petri dishes. (G) Cells were mixed with bacteria and spread on SM/5plates and the cell numbers were counted at the indicated time points. (H) Cells were inoculated at a density of 1×10^6 cells/ml in FM minimal media and cell density was measured every day. (I) Ax2 and *pkcA*$^-$ cells were treated with 0.15μg/ml ScPPX1 or buffer and a proliferation assay was performed. (J) Proliferation assay was performed in 2X and 0.5X along with 1X HL5 and the cell density was measured every day. The proliferation curves of *pkcA*$^-$ cells grown in 2X, 1X and

0.5X HL5 were compared to those of Ax2 grown in 2X, 1X and 0.5X HL5 respectively. (K) Proliferation assay of Ax2 and *pkcA*$^{-}$ cells overexpressing Coronin A. The growth curve of *pkcA*$^{-}$/*CorA*-OE cells was similar to Ax2/*CorA*-OE. All values are mean ± SEM; n=3 independent experiments and were analyzed using two-way ANOVA with Bonferroni's multiple comparisons for all the graphs. ****p<0.0001,***p<0.001,**p<0.01, *p<0.05. and ns-not significant.

Fig. S2. CM treatments.

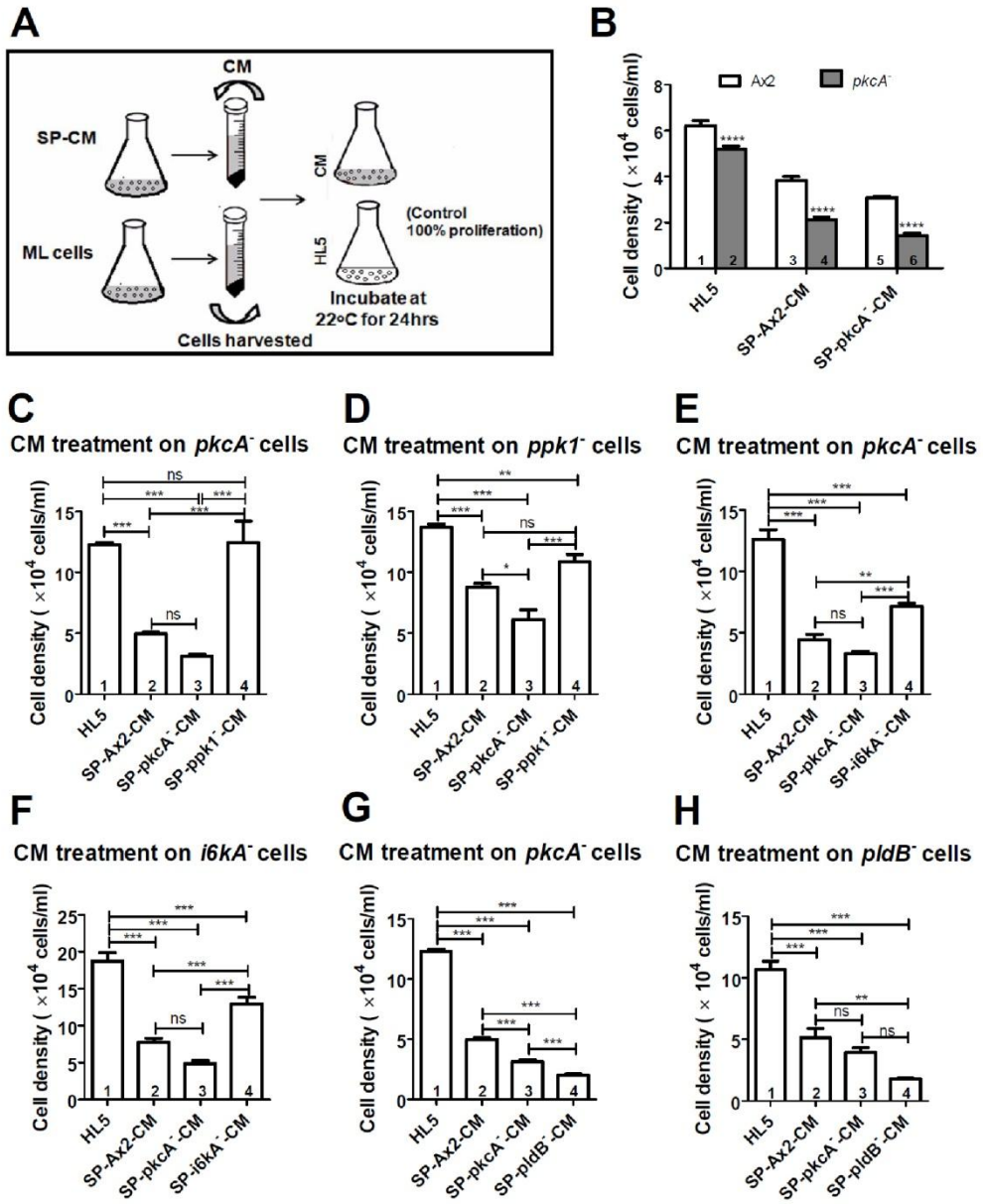

Fig. S2. CM treatments. (A) Schematic representation of the experimental design to study the effect of CM on proliferation in shaking conditions. (B) Ax2 and *pkcA*$^-$ cells were treated with their respective SP-CM from shaking cultures, incubated at 22°C for 24 h with constant shaking (150 rpm) and after 24 h the cells were counted using a hemocytometer. Bar 1 and 2: Control. Ax2 and *pkcA*$^-$ cells grown in HL5 while testing SP-CM; bar 3 and 4: CM was collected from Ax2 cultures after they reached the maximum cell density (SP density; 20-25x10^6 cells/ml). This CM was tested on Ax2 and *pkcA*$^-$ cells; bar 5 and 6: CM was collected from *pkcA*$^-$ cultures after

they reached the maximum cell density (SP density; 10-15x10^6 cells/ml). This CM was tested on Ax2 and *pkcA*$^-$ cells. (C) To know whether the CM with reduced polyP can rescue *pkcA*$^-$ proliferation, *pkcA*$^-$ cells were treated with SP-CM from SP-*ppk1*$^-$-CM. (E) *PkcA*$^-$ cells were treated with SP-*i6kA*$^-$-CM to check if the proliferation defect can be rescued. (G) Addition of SP-*pldB*$^-$-CM to *pkcA*$^-$ to determine the extent to which proliferation is inhibited. (D, F and H) Addition of SP-*pkcA*$^-$-CM to *ppk1*$^-$ (D), *i6kA*$^-$ (F) and *pldB*$^-$ (H) to know the extent to which proliferation is inhibited. The testing was done on *pkcA*$^-$ cells (C, E and G), *ppk1*$^-$ (D), *i6kA*$^-$ (F) and *pldB*$^-$ (H). Bar 1: Control: *pkcA*$^-$ (C, E and G), *ppk1*$^-$ (D), *i6kA*$^-$ (F) and *pldB*$^-$ (H) cells grown in HL5; bar 2: CM was collected from Ax2 cultures after SP density was reached. bar 3: CM was collected from *pkcA*$^-$ cultures after they reached the maximum cell density. bar 4: CM was collected from *ppk1*$^-$(C and D), *i6kA*$^-$ (E and F) and *pldB*$^-$(G and H) cultures after they reached the maximum cell density. Data are means ± SEM from n=3 biologically independent samples. Statistical significance was assessed by two-way ANOVA with Bonferroni's multiple comparisons (B) and one-way ANOVA with Tukey's multiple comparisons (C-H). . ***p<0.001, **p<0.01and *p<0.05.

Fig. S3. The secreted factors AprA and CfaD are not responsible for the growth defect in *pkcA*⁻ cells.

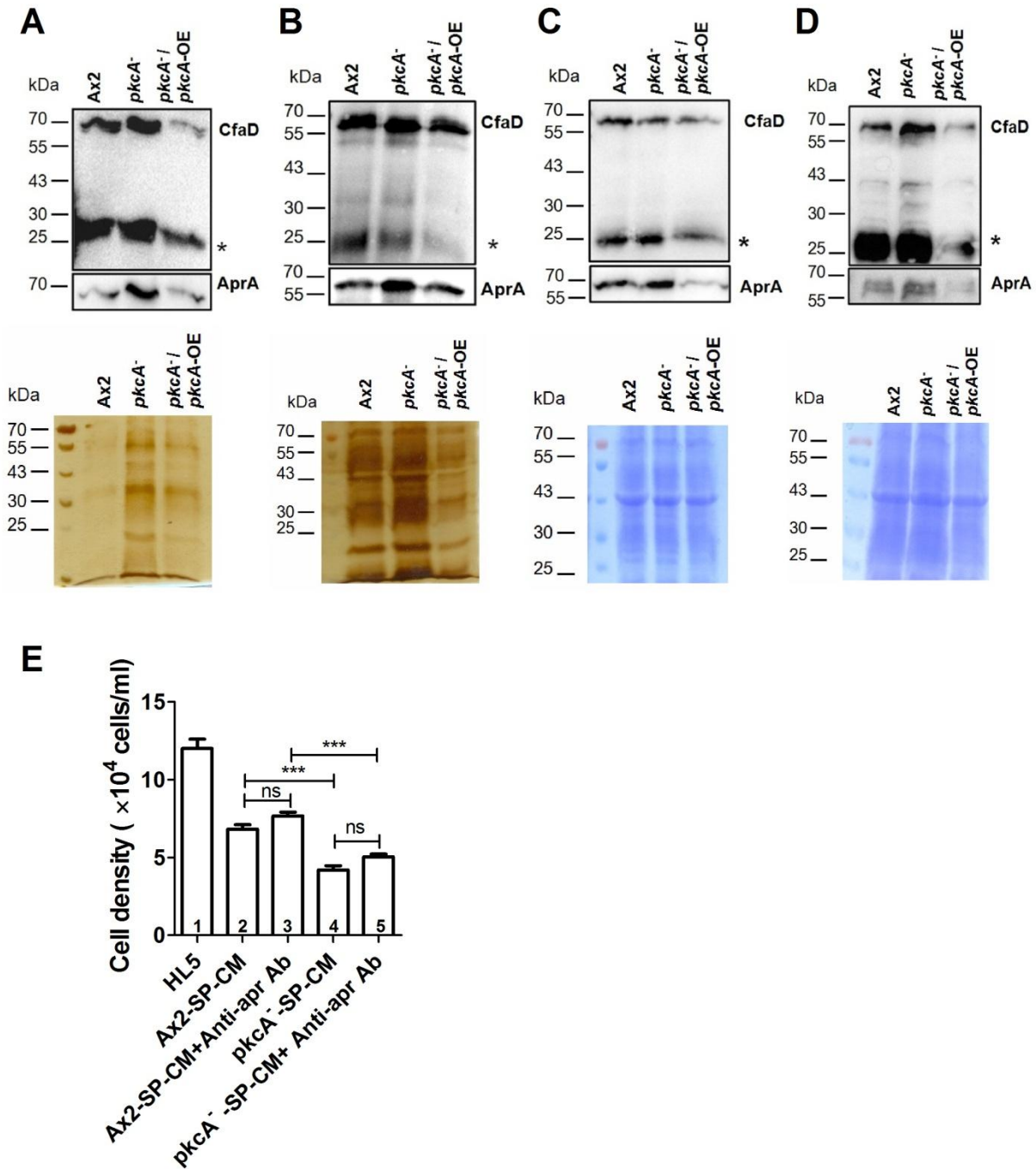

Fig. S3. The secreted factors AprA and CfaD are not responsible for the growth defect in *pkcA*⁻ cells. (A and B) To check if the levels of these two autocrine factors were abnormal in *pkcA*⁻, ML-CM (A) and SP-CM (B) from Ax2, *pkcA*⁻ and *pkcA*⁻/*pkcA*-OE were collected and the extracellular levels of AprA and CfaD were examined by western blotting. Note that total protein

levels are high in *pkcA*$^{-}$ cells in both ML and SP CM. Images are representative of three independent experiments. (C and D) ML (C) and SP (D) cells were collected and the intracellular levels of AprA and CfaD were examined by western blotting. (E) To ascertain if the inhibitory activity of SP-*pkcA*$^{-}$-CM is due to excess AprA, the CM was treated with anti-AprA antibody (1:150) and thereafter, cell proliferation was examined in Ax2 and *pkcA*$^{-}$ cells. Surprisingly, there was no difference in the proliferation rates in both cell types suggesting that high aprA levels in ML- *pkcA*$^{-}$-CM do not contribute to the defective growth of the mutant. The CMs were tested on Ax2 cells. Bar 1: Control. Ax2 cells grown in HL5 while testing SP-CM; bar 2 and 4: CM was collected from Ax2 and *pkcA*$^{-}$ culture after they reached the maximum cell density. bar 3 and 5: CM was collected from Ax2 and *pkcA*$^{-}$ cultures after they reached the maximum cell density. This CM was treated with anti-AprA antibody. Data are means ± SEM; n≥3 biologically independent experiments. Statistical significance was assessed by one-way ANOVA with Tukey's multiple comparisons. ***p<0.0001 and ns-not significant.

Fig. S4: Extensive variation of extracellular polyP levels in pinocytosis mutants.

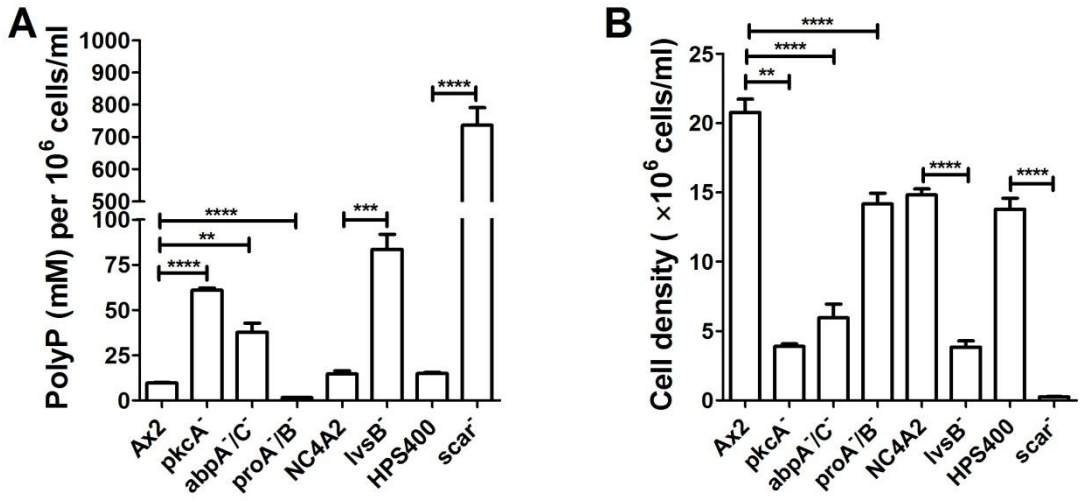

Fig. S4. Extensive variation of extracellular polyP levels in pinocytosis mutants. (A) Mutants and parental strains were grown in FM media and the stationary phase cell densities were recorded. (B) Extracellular CM from the cells were collected at the SP cell density, polyP concentration was estimated and normalized to respective SP cell density. All data represents means ± SEM from n=3 independent experiments. For each strain, the data was analyzed using two-tailed paired *t*-test and compared to parental strains. The polyP levels and SP densities of *pkcA*$^-$, *abpA*$^-$*/C*$^-$ and *proA*$^-$*/B*$^-$ were compared to those of Ax2 (Ax2-214 (DBS0235534); *lvsB*$^-$ to NC4A2 and *scarA*$^-$ to HPS400. **** p<0.0001, *** p<0.001 and ** p < 0.01.

Fig. S5. Cell cycle analysis of *pkcA*⁻ cells suggest large fraction to be multinucleate in shaking conditions.

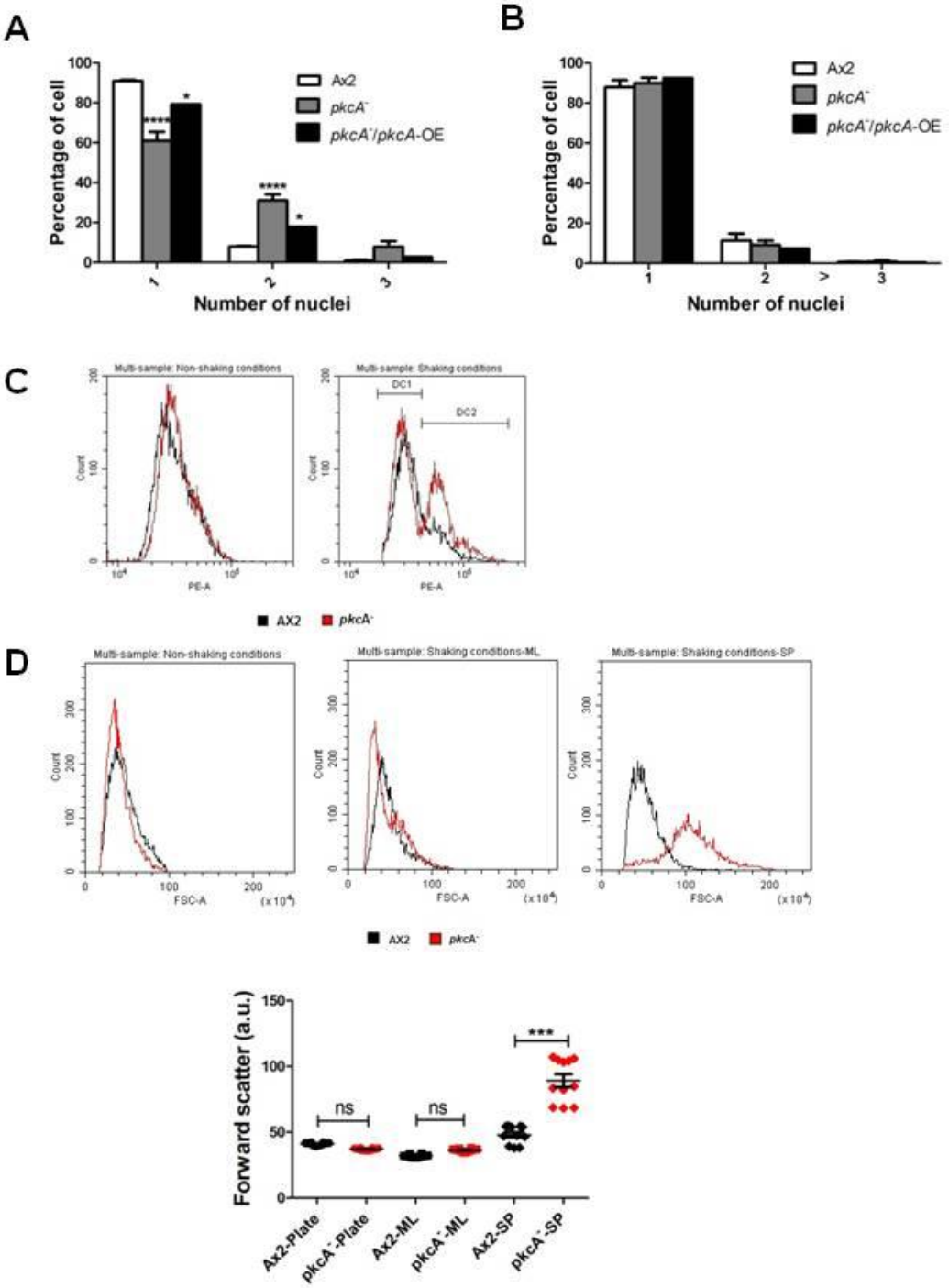

Fig. S5. Cell cycle analysis of *pkcA*$^-$ cells suggests a large fraction are multinucleate in shaking conditions. (A, B) Nuclear content of cells grown in shaking conditions (A) and Petri dishes (B), at least 100 cells were analyzed per experiment; n=3. (C) Cell cycle analysis was carried out using a flow cytometer (CytoFLEX apparatus, Beckman-Coulter, USA) with propidium iodide stained Ax2 and *pkcA*$^-$ cells grown in shaking and non-shaking conditions. The cell cycle phases of both Ax2 and *pkcA*$^-$ cells were almost identical except that in the G2 phase of *pkcA*$^-$ cells, there were two peaks, indicating a fraction of multinuclear cells. (D) Forward scatter of Ax2 and *pkcA*$^-$ cells grown in shaking and non-shaking conditions. For flow cytometry, 10,000 events per experiment were considered. All data represents means ± SEM from n=3 independent experiments and analyzed using two-way ANOVA with Bonferroni's multiple comparisons (A and B) and one-way ANOVA with Tukey's multiple comparisons (D). ****p0.0001, ***p<0.001, *p0.05 and ns- not significant.

Fig. S6: Early stationary phase entry in *pkcA*⁻ cells are not due to myosin II defects.

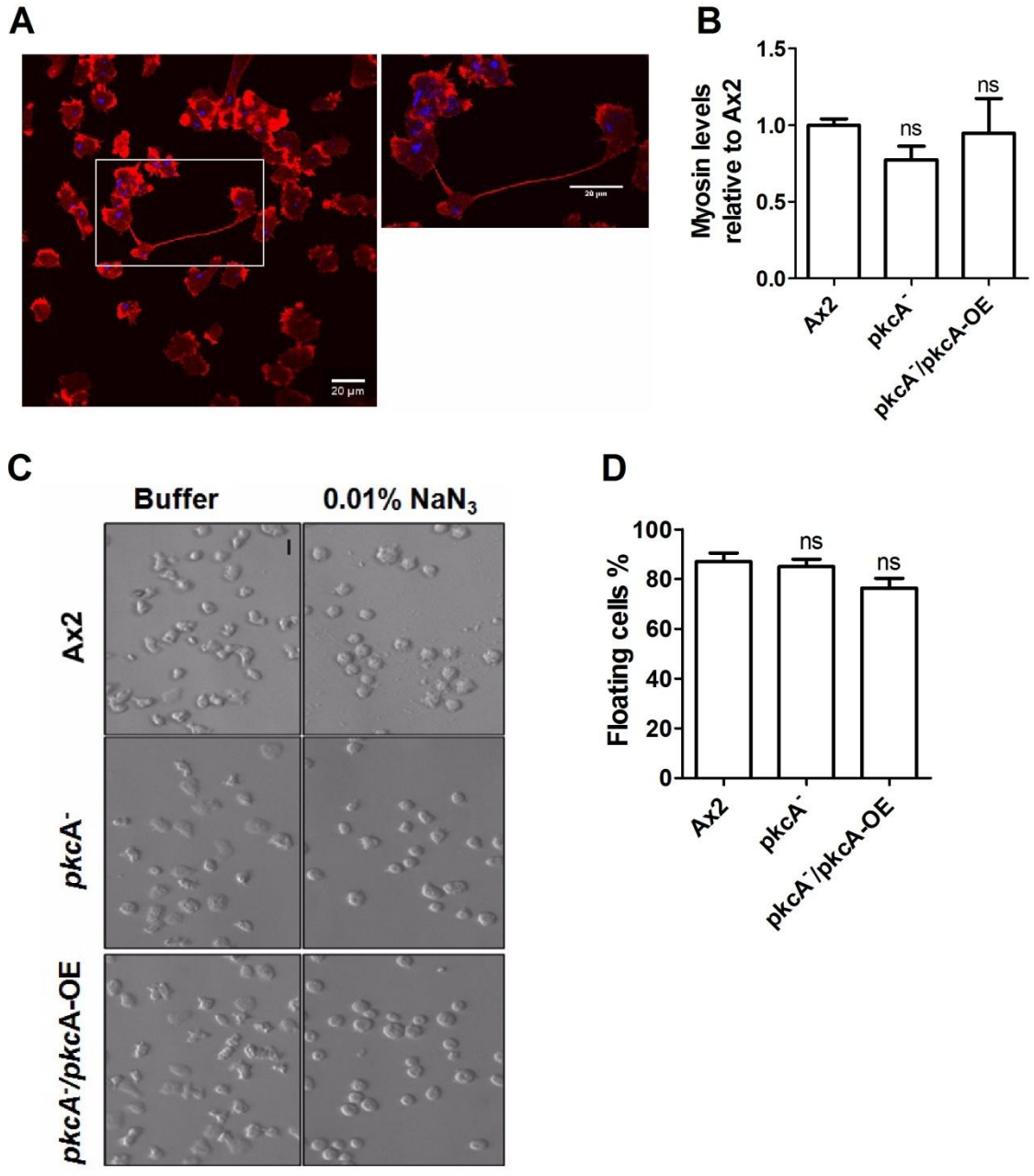

Fig. S6. Early stationary phase entry in *pkcA*⁻ cells are not due to myosin II defects. (A) Similar to *pkcA*⁻, *Dictyostelium* mutants defective in myosin II assembly also show SP entry at a reduced cell density and such impaired growth was not reported when grown in plates (Wang et al., 2011). The multinucleated *pkcA*⁻ cells grown in shaking conditions when transferred to a glass surface go through traction-mediated cytofission like myosin II defective mutants. A

representative image is shown. (B) To examine if the *pkcA*$^-$ growth defects were associated with a myosin II defect, assembled myosin levels were measured in the cytoskeletal fraction of ML cells grown in suspension and normalized to total protein levels. There was no significant difference in the myosin II levels of *pkcA*$^-$ and Ax2 cells. (C and D) Myosin II activity was examined after treating ML *pkcA*$^-$ and Ax2 cells with 0.01% sodium azide for 30 min and the fraction of floating versus adhered cells was counted. Surprisingly, there was no significant difference in the fraction of floating versus adhered cells in Ax2 and *pkcA*$^-$ cells. These results suggesting that myosin II assembly or its function do not contribute to the growth defect of *pkcA*$^-$. Data are means ± SEM; n≥3 biologically independent experiments. Statistical significance was assessed by one-way ANOVA with Tukey's multiple comparisons (B and D). ns-not significant.

Fig. S7. PkcA-GFP localization in lysosomal vesicles and PkcA regulates lysosome dependent processes.

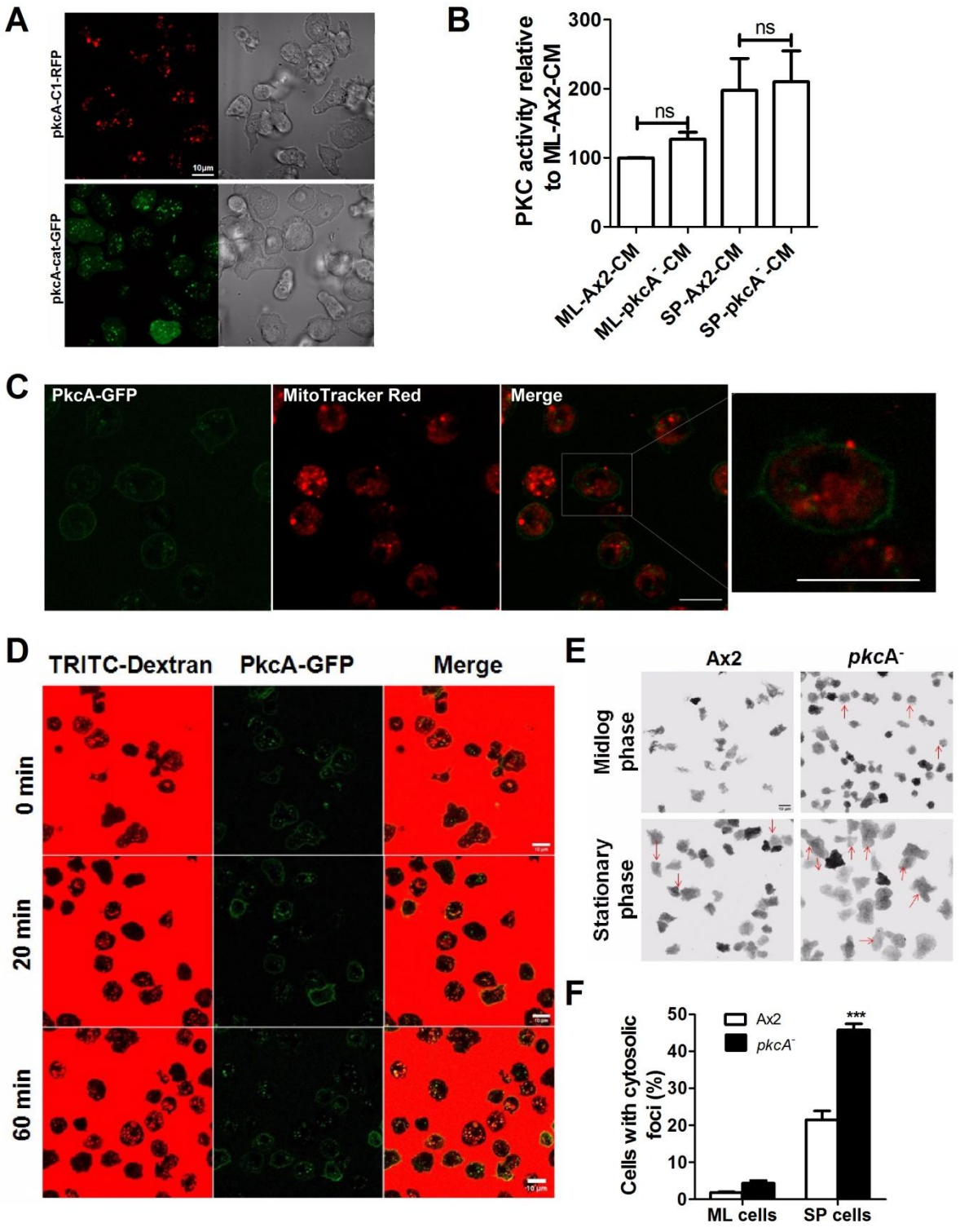

Fig. S7. PkcA-GFP localization in lysosomal vesicles and PkcA regulates lysosome dependent processes. (A) Representative images showing regulatory C1 domain (pkcA-C1-RFP) and catalytic kinase domain (pkcA-cat-GFP) localization in Ax2 cells. Scale bar -10µm. (B) A PKC activity assay was performed in ML and SP CM. The activity is normalized to ML-Ax2-CM. Data are means ± SEM; n=3 biologically independent samples. Statistical significance was determined using a one tailed paired *t*-test. ns-not significant. (C) PkcA-GFP containing cells were treated with MitoTracker Red and visualized by confocal microscope. Scale bar -10µm. (D) PkcA-GFP containing cells were incubated with 2mg/ml TRITC-dextran and imaged at the indicated time points. Scale bar -10µm. Scale bar- 10µm. (E and F) *PkcA*$^{-}$ cells have higher protein aggregation. Image of GFP spots (E) and Quantification of GFP spots (representing polyQ foci) (F). At least 50 cells were analyzed per experiment. Scale bar- 10µm. Data represents means ± SEM from n=3 independent experiments. In E, statistical significance was determined using a one tailed paired *t*-test. ***p<0.001.

Fig. S8. *PkcA* regulates *i6kA* expression levels.

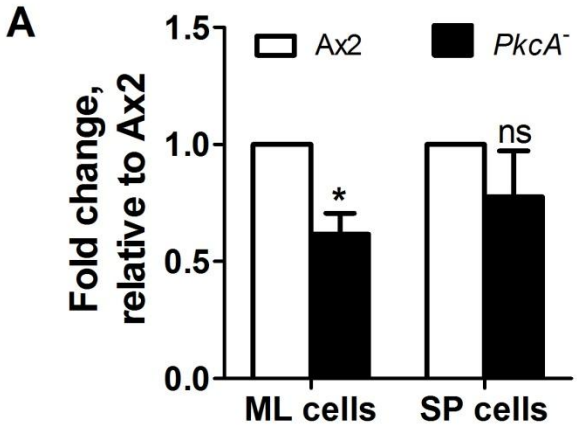

B

* x-[S/T]-x-[R/K]- Consensus PKC phosphorylation site

		Netphos 3.1 prediction score
9 S	YLVNSKKSK	0.860
572 S	PSNRSTRSN	0.864

Fig. S8. PkcA regulates *i6kA* expression levels. (A) qRT-PCR for *i6kA* gene expression in ML and SP cells. Data are means ± SEM; n=3 biologically independent samples. Statistical significance was assessed by one tailed paired *t*-test. *p<0.05 and ns-not significant. (B) Probable PKC phosphorylation sites in i6kA protein sequence determined using NetPhos 3.1.

Fig. S9. SDS-PAGE gel images used to quantify F-actin and Myosin levels.

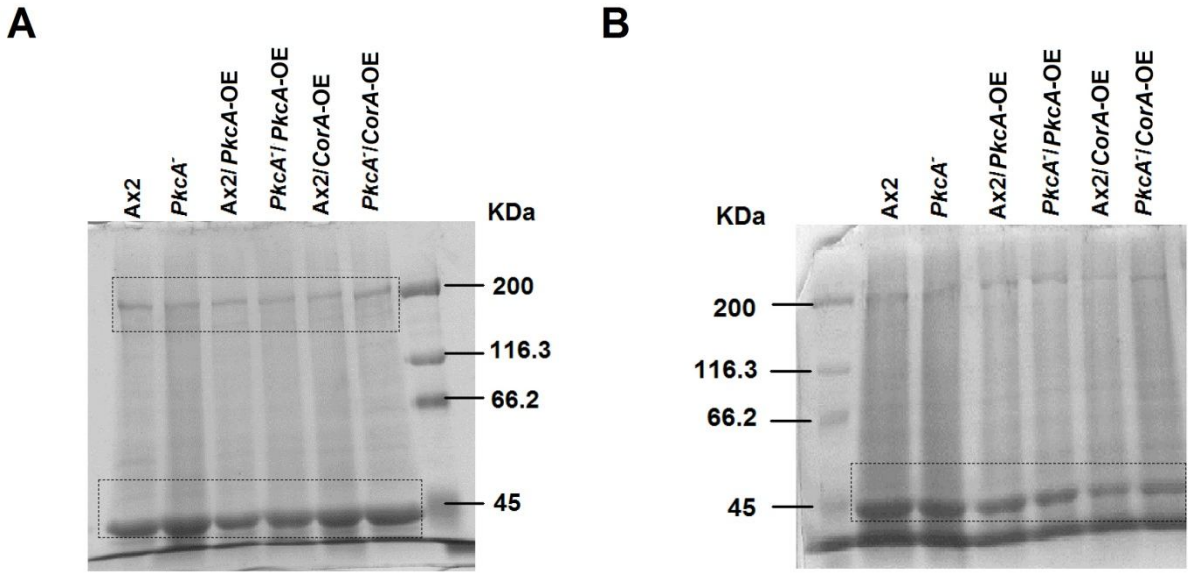

Fig. S9. SDS-PAGE images were used to quantify F-actin and myosin levels. Cytoskeletal fraction from cells grown in (A), shaking and (B), non-shaking conditions. The solid line box indicates assembled myosin bands and the dashed line box indicates F-actin bands. Refer Fig.6B,CD for F-actin quantification graph and Fig. S6B for myosin quantification graph

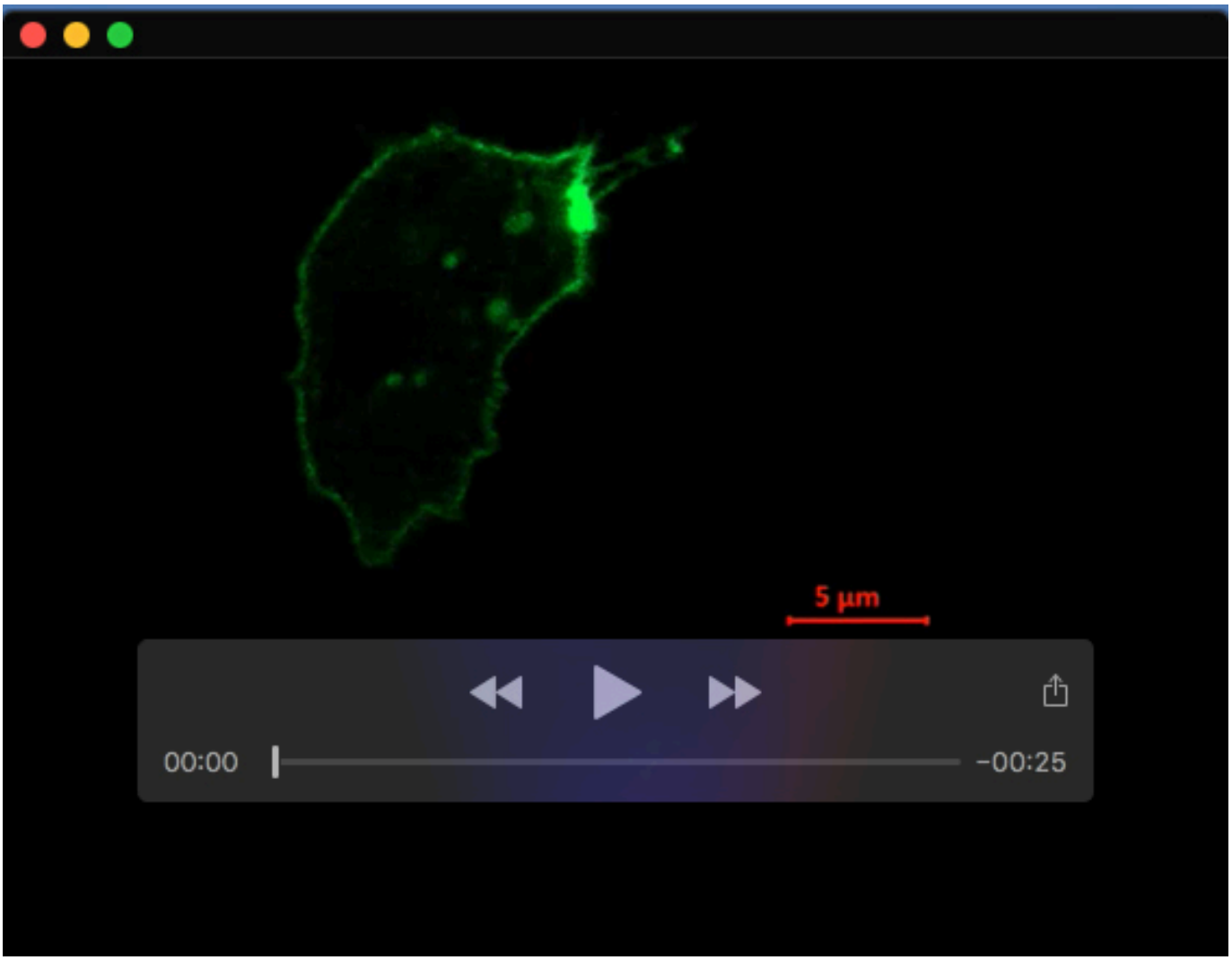

Movie 1. PkcA-GFP is localized to vesicles and the plasma membrane.

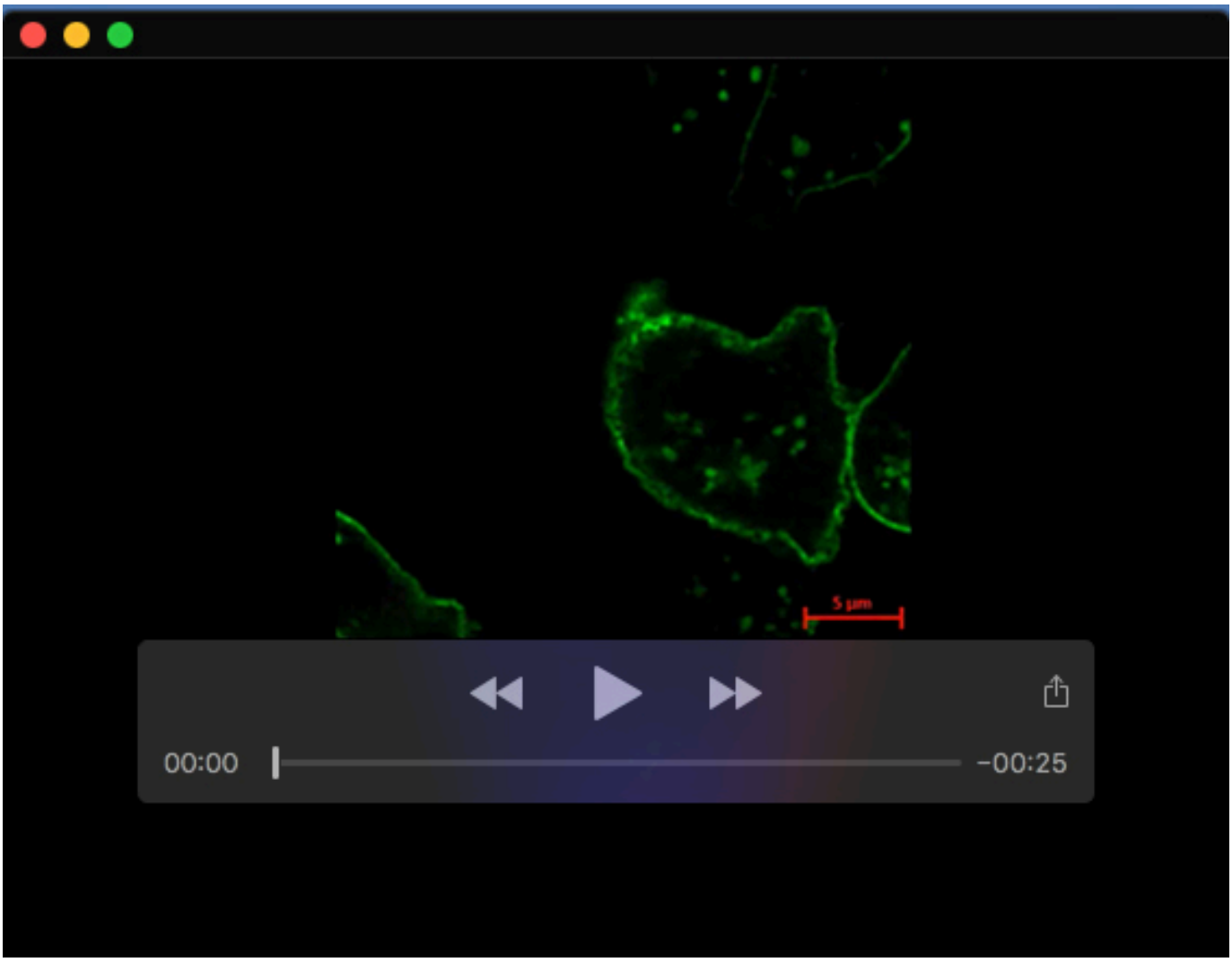

Movie 2. PkcA-GFP in motile cells. In motile cells, PkcA-GFP was accumulated to the rear end.

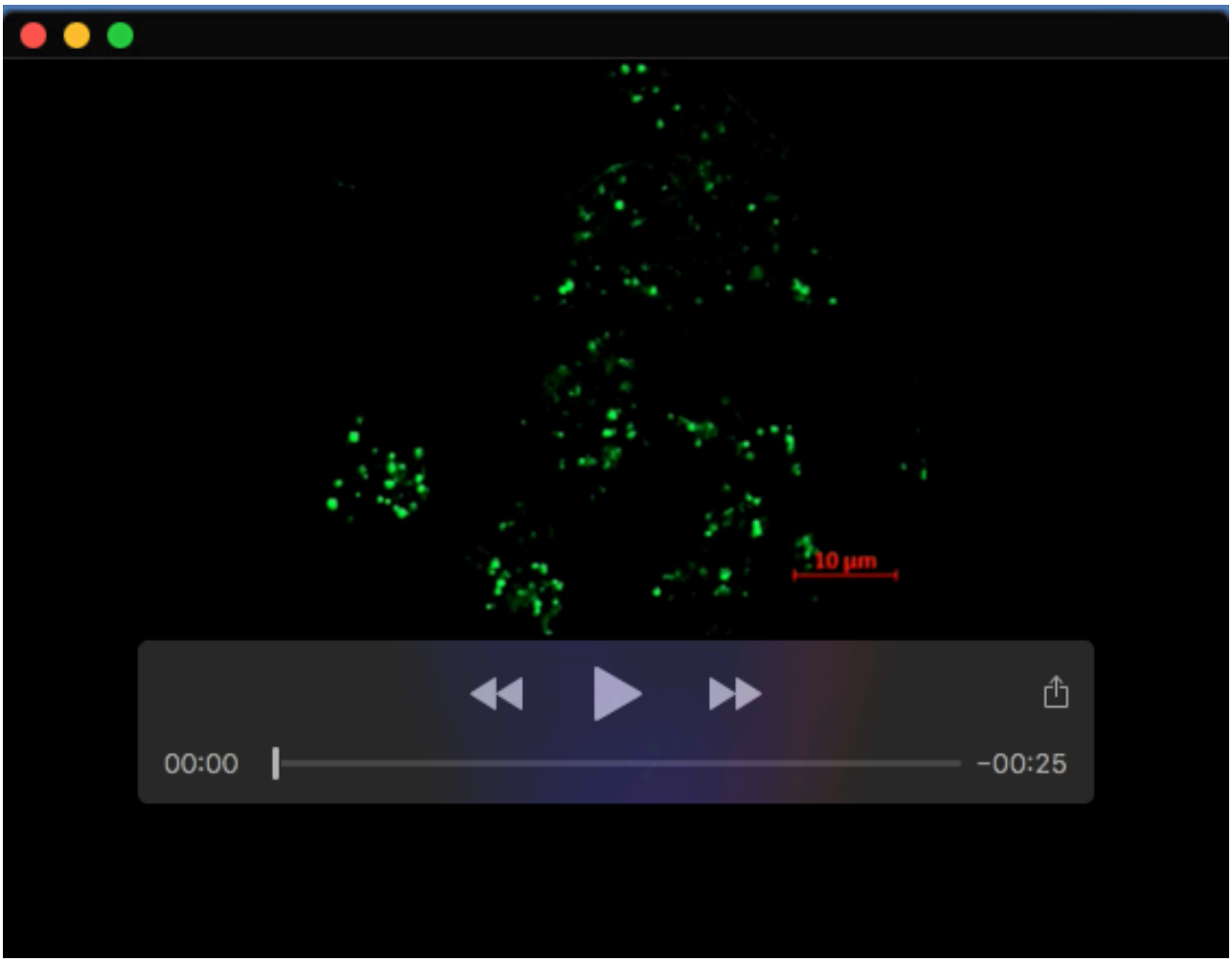

Movie 3. PkcA localization is not affected by DMSO (control)

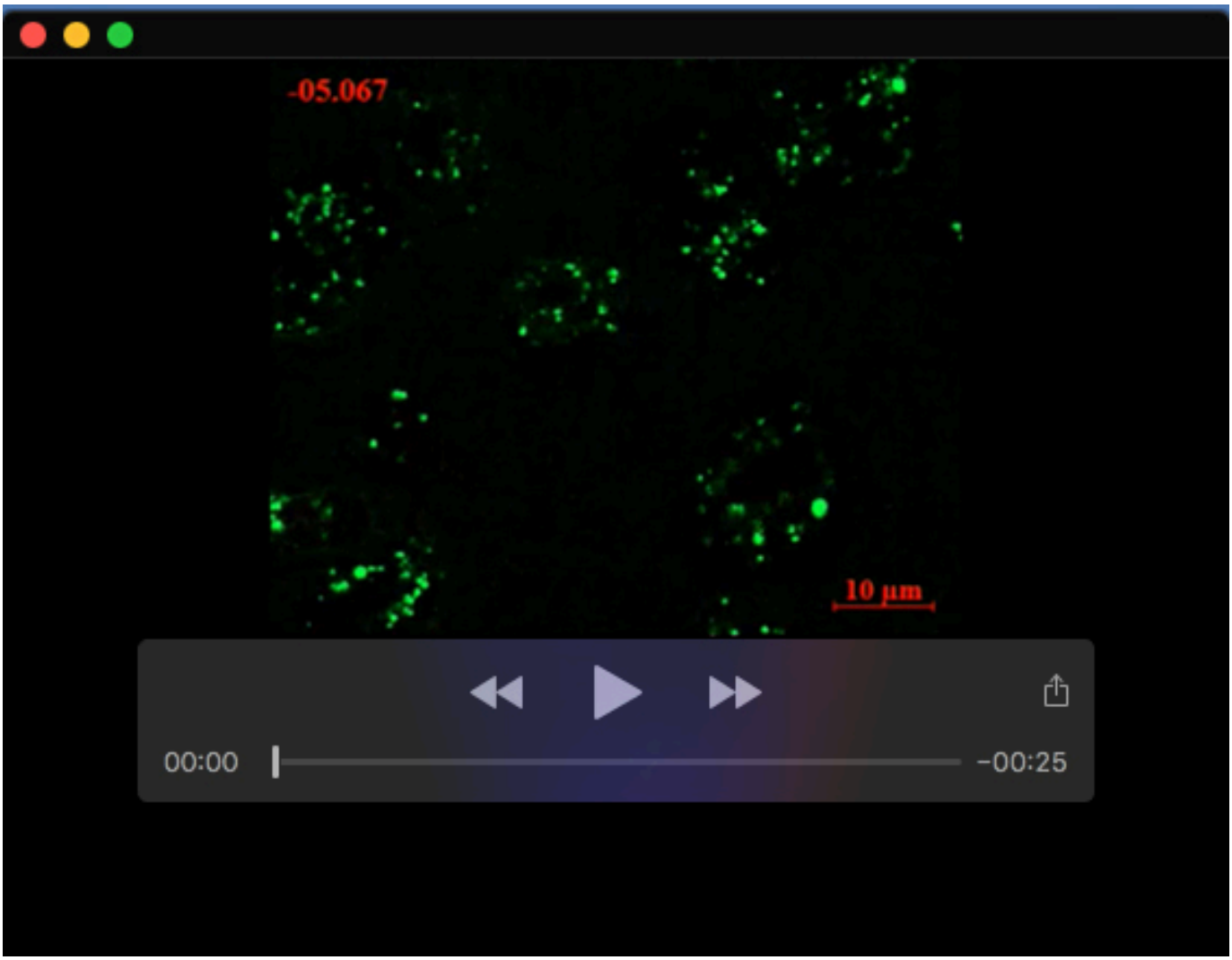

Movie 4. PkcA-GFP localization is not affected by PKC activity. To ascertain if the PKC activity is required for pkcA-GFP localization, Ax2/*act*15::*pkcA*-GFP cells were treated with 10 µM Bis I and pkcA-GFP localization was visualized.

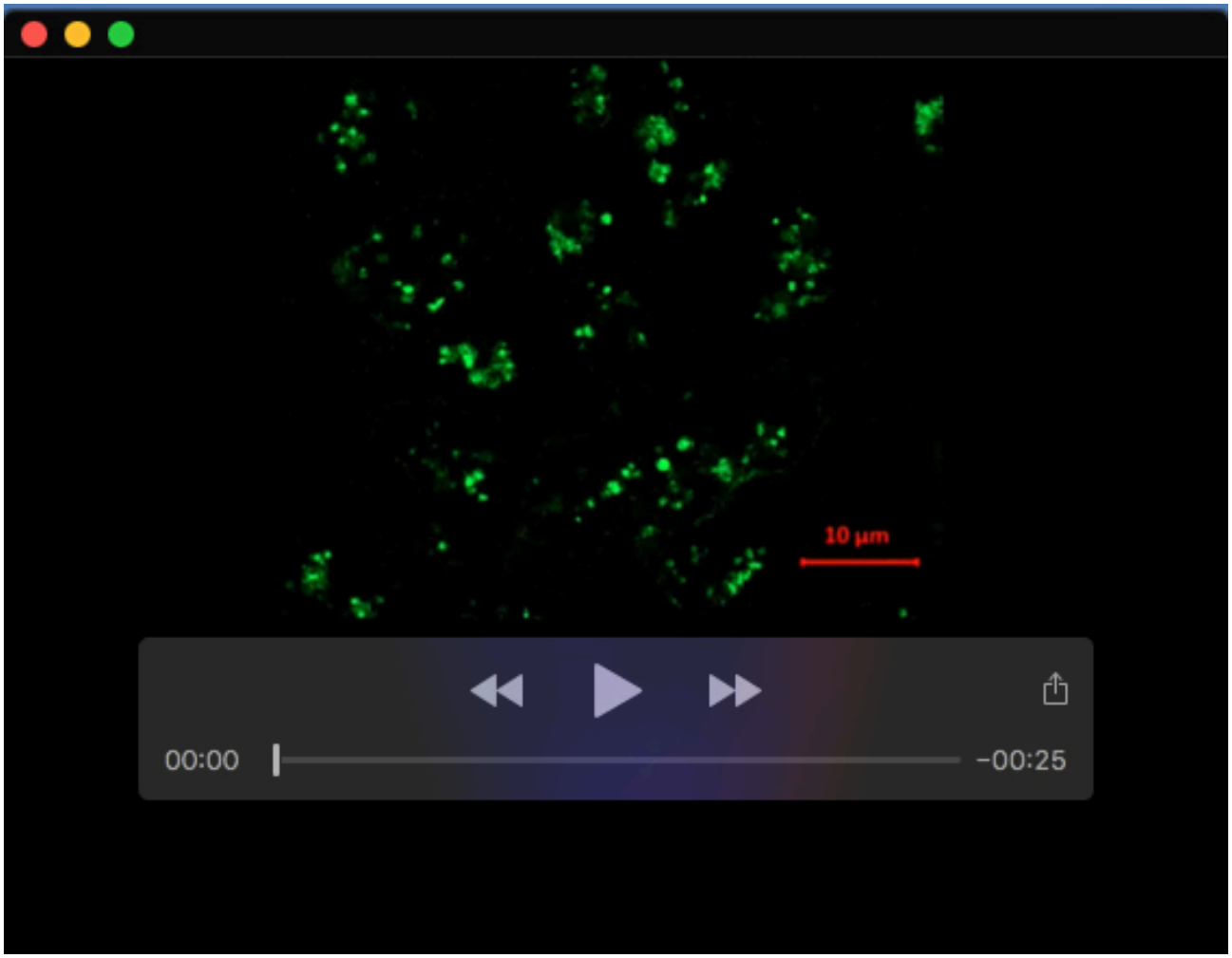

Movie 5. Actin polymerization is important for pkcA-GFP containing vesicular movement. To ascertain if actin polymerization is important for pkcA-GFP movement, Ax2/*act*15::*pkcA*-GFP cells were treated with 10 µM Latrunculin B and pkcA-GFP localization was visualized. Lat B treated cells round up and although the membrane localization of pkcA-GFP was intact, pkcA-GFP containing vesicles clutter together and showed no further movement. Thus, for vesicular pkcA-GFP localization actin polymerization is important.

Table S1. Stationary phase cell density in different conditions.

Conditions		Maximum observed cell density (× 10^6 cells/ml)	
		Ax2	***pkcA*⁻**
Growth assay[a]		25.1 ±1.2	12.6±0.4 ***
Growth of SP- *pkcA*⁻ cells in fresh HL5[b]	Initial SP cell density	22.6±1.1	13.8±0.6*
	In fresh HL5 (at the SP cell density)	44.8±2.4	24.2±2.5****
	In CM (at SP cell density)	20.1±4.0	6.9±1.8****
	In fresh HL5 (at ¼ th of SP cell density)	23.1±1.1	13.4±0.7**
	In CM (at ¼ th of SP cell density)	6.2±0.9	4.5±0.6^{ns}
Initial cell density[b]	1×10^5 cells/ml	20.4±1.2	13.6±0.8***
	5×10^5 cells/ml	17.9±1.2	10.6±1.0**
	1×10^6 cells/ml	18.7±1.8	13.8±0.9*
Rotation speed[b]	50 rpm	4.8±0.3	5.2±0.9^{ns}
	100 rpm	14.2±1.4	10.3±0.4**
	150 rpm	19.9±0.7	12.0±0.6****
Flask size[b]	25ml	18.5±0.8	12.7±1.0*
	50ml	22.0±1.4	14.2±0.2**
	100ml	20.0±1.8	12.6±2.5**
ScPPX1 treatment[b]	Control	19.6±2.3	14.0±0.4*
	0.15µg/ml ScPPX1	37.5±2.0	24.8±2.9**
CorA overexpression[b]	Controls	25.2±0.8	13.9±0.4***
	CorA-OE	23.8±1.53	22.30±1.04^{ns}
Different concentrations of HL5 media[b]	0.5X	4.0±0.5	3.3±0.7^{ns}
	1X	21.8±1.2	13.8±0.3**
	2X	26.4±2.2	23.0±2.5^{ns}

SP cell density upon Bis I treatment[a]**.**	
Bis I treatment	**Maximum observed cell density, ×10^6 cells/ml**
Ax2	21.4±0.6
pkcA⁻	12.7±0.4***
Ax2 + 1 µM Bis I	17.1±0.6***,###
Ax2 + 3 µM Bis I	17.5±0.7***,###
Ax2 + 5 µM Bis I	14.1±0.6***,ns
Ax2 + 10 µM Bis I	11.9±0.8***,ns
Ax2 + 20 µM Bis I	10.1±0.6***,ns
Ax2 + 40 µM Bis I	10.4±0.3***,ns
pkcA⁻ + 5 µM Bis I	12.4±0.1^{ns}
pkcA⁻ + 10 µM Bis I	11.1±0.5$^{\#}$
pkcA⁻ + 20 µM Bis I	10.9±0.2$^{\#\#}$
pkcA⁻ + 40 µM Bis I	10.3±0.3$^{\#\#\#}$
SP cell density of strains carrying individual domains of pkcA[a]**.**

Cell type	Maximum observed cell density, $\times 10^6$ cells/ml
Ax2	25.0±0.2
pkcA$^-$	10.8±1.6***
pkcA$^-$/ *pkcA*-C1	10.8±0.6***
pkcA$^-$/ *pkcA*-Cat	10.8±1.3***
pkcA$^-$/*pkcA*-OE	18.6±2.1^{ns}

[a]one- way ANOVA with Tukey's multiple comparisons
[b]two-way ANOVA with Bonferroni's multiple comparisons
Comparison with Ax2 are represented as ****p<0.0001,***p<0.001,**p<0.01, *p<0.05. and ns-not significant. Comparison with *pkcA*$^-$ are represented as $^{###}$ p<0.001, ,$^{##}$p<0.01, $^{#}$p<0.05. and ns-not significant.

Table S2. SP cell density and polyP levels in pinocytosis and exocytosis defective mutants

Cell type	Maximum observed cell density, $\times 10^6$ cells/ml	PolyP levels /10^6 cells
Ax2	20.8±0.9	9.6±0.4
PkcA$^-$	3.9±0.2[a]	60.9±1.3[b]
AbpA$^-$/*C*$^-$	5.9±1.0[b]	37.8±4.9[a]
ProA$^-$/*proB*$^-$	14.2±0.8[b]	1.6±0.1[b]
NC4A2	14.8± 0.4	14.7±1.7
LvsB$^-$	3.8±0.4[c]	83.5±8.3[d]
HPS400	13.8 ±0.8	14.9 ± 0.8
ScarA$^-$	0.2 ±0.02[e]	736.7 ± 54.3[e]

[a] $p<0.01$ compared with Ax2(two-tailed paired *t*-test).
[b] $p<0.0001$ compared with Ax2(two-tailed paired *t*-test).
[c] $p<0.0001$ compared with NC4A2 (two-tailed paired *t*-test).
[d] $p<0.001$compared with NC4A2 (two-tailed paired *t*-test).
[e] $p<0.0001$ compared with HPS400(two-tailed paired *t*-test).